1967

The image-dissector, multiplier phototube as a detector in analytical emission spectroscopy

Danold Wayne Golightly
Iowa State University

GOLIGHTLY, Danold Wayne, 1941-
THE IMAGE-DISSECTOR, MULTIPLIER PHOTOTUBE AS A DETECTOR IN ANALYTICAL EMISSION SPECTROSCOPY.

Iowa State University, Ph.D., 1967
Chemistry, analytical

University Microfilms, Inc., Ann Arbor, Michigan

THE IMAGE-DISSECTOR, MULTIPLIER PHOTOTUBE AS A DETECTOR IN ANALYTICAL EMISSION SPECTROSCOPY

by

Danold Wayne Golightly

A Dissertation Submitted to the
Graduate Faculty in Partial Fulfillment of
The Requirements for the Degree of
DOCTOR OF PHILOSOPHY

Major Subject: Analytical Chemistry

Approved:

Signature was redacted for privacy.

In Charge of Major Work

Signature was redacted for privacy.

Head of Major Department

Signature was redacted for privacy.

Dean of Graduate College

Iowa State University
Of Science and Technology
Ames, Iowa

1967

TABLE OF CONTENTS

I. INTRODUCTION

Because of the intrinsic ease and convenience afforded by electrical measurements, there has long been a general trend for analytical chemists to employ instrumental techniques in order to solve a wide range of analytical problems. The chemical literature attests this trend and furthermore, provides a picture of increasing sophistication of equipment and growing concern of the experimentalist over the basic operational characteristics of existing equipment. At times, observations of deficiencies or limitations of a particular technique have given birth to new ideas and measuring apparatus which have extended the working tools and capabilities of the analytical chemist. A particular example of such an event is embodied in the details of the recently developed "p-metal" electrodes. A somewhat "casual" observation of the interference produced by high concentrations of alkali metal ions on the electrometric determination of pH with glass electrodes in aqueous solutions has resulted in the production of electrodes that are selectively responsive to a number of solvated metal ions.

Although every such observation and reassessment cannot lead to a profound result, there is the continuing hope that

a constant re-evaluation process will generate greater understanding, and that new ideas will improve the present instrumentation and techniques.

Direct-reading spectroscopy refers to the spectroscopic-electronic technique of rapid chemical analysis which employs electron multiplier phototubes to obtain measurements of relative spectral line intensities and automatically relates this intensity information to the quantities of each of the elements which produce the line radiations. This method of analysis is now an accepted and integral part of rapid, economical control methods in much of the metallurgical and chemical industries and has proven to be very successful for the accurate and precise analyses of large numbers of similar samples within short time intervals.

Many variations of the basic components of instrumentation have been used, however one general assembly scheme is common. Optical radiation from a source which is capable of exciting atomic emissions, such as an arc, spark or flame, is dispersed by a prism or grating spectrograph. The luminous flux which passes through each exit slit then is directed onto the cathode surface of a photomultiplier tube, and the resulting photocurrent is stored on a capacitor. Since the

magnitude of this photocurrent is directly proportional to the relative intensity of a spectral line, the potential across the capacitor, which is dependent upon the capacitance and charge (or time-integrated current), is a direct function of the relative peak intensity of the spectral line observed. Thus, line intensity ratios can be determined as rapidly as the potentials which correspond to line and background intensities can be measured, and related to analyte concentrations from comparisons with initial calibration information.

The degree of success of such methods in providing both accurate and precise element analyses is critically dependent on a number of factors. Exit slits must be positioned along the spectrograph focal plane with tolerances of the order of a few microns and maintained in a fixed alignment with the spectrum at least for the duration of the integration period. The difficulty in performing such a task is a function of the dispersion of the spectrograph and complexity of the spectra encountered. Commonly, some spectral lines, which are analytically useful, lie so close to one another that separation by means of the exit slits is not possible. In light of the intended objective to do many analyses on similar samples, long term stability of the system is desired. Diverse effects

attributable to thermal expansion and contraction of the slit mounting bar and slits may be minimized by thermostating the spectrograph or room that contains the spectrograph. This temperature control also alleviates the problem of asymmetric shifts of the spectrum due to expansion and contraction of the grating. Atmospheric pressure and humidity changes which affect air density and thus refractive index are not so readily controlled. Sawyer (1, pp. 186-189) has provided some explicit information on the magnitude of the effects of temperature and pressure variations with regard to the grating and air density. The concurrent expansion and contraction of both the grating and air by temperature changes produce effects that partially tend to balance one another. For a temperature increase, the first effect causes a shift of the spectrum toward shorter wavelengths because of the dispersion decrease that occurs in direct proportion to the grating constant and expansion of the rulings. However, expansion of the air within the spectrograph produces an increase of the wavelength of the spectral lines. For gratings ruled on quartz, the primary effect of temperature on the spectral line position is attributable to changes in air density. Shifts that result from grating variations are about

10^{-6} Å/°C and those from air density changes are approximately 3×10^{-3} Å/°C. Thus, for a spectrograph with a first-order, reciprocal linear dispersion of 5 Å/mm, a spectrum position change of 0.6 μ/°C should be expected. Correspondingly, at the 5000 Å location for the same spectrograph, a spectrum position change of 0.4 μ/mm Hg should be anticipated. However, a shift of about 1.8 μ for a 1 percent change in relative humidity has been calculated. Since exit slits of 50 μ width commonly are employed along the focal plane of a direct-reading spectrograph, the importance of temperature, pressure, and humidity changes becomes very apparent. Serious nonlinearity in potential readings occurs if charge levels on a capacitor exceed about 10 percent of the applied voltage (2). In addition, the integration periods must be highly reproducible, and the dc-coupled, electronic, integrating circuitry must demonstrate very little drift. Naturally, with arc or spark discharges, the usual considerations of matrix effects, excitation conditions, electrode shapes and line selections must be observed.

In modern direct-reading equipment, the correction for spectral background also presents a serious problem. Spectral background refers to continuous radiation which is present

under the spectral line of interest and is not characteristic of the element which produces the spectral line. Intensity measured at the exit slit is the sum of the line and background intensities, and background intensity must be subtracted from this total in order to obtain the true line intensity. Such corrections are accommodated in current direct-reading instruments through two different approaches. One method utilizes separate phototubes to measure the background adjacent to the spectral line. This measurement is commonly made only on one side of the line, however greater accuracy is attained through use of an average value from measurements on both sides of the line. One or two additional phototubes are required for each spectral line, and background exit slits must be positioned close enough to the exit slit for the spectral line to permit accurate background measurements. Generally, these requirements are difficult to meet and add to the complexity of the instrument. Another method employs a blank sample (analyte elements absent) for determination of background. The blank sample is excited under conditions identical to those intended for the unknown sample, and the corresponding background signal at the exit slit is measured. This intensity value is then subtracted from all

the subsequent measurements on the spectral line. Since the background signal may change with variations in the sample composition, this method does not always give satisfactory results. In addition, this technique requires very high stability in the measuring electronics.

Other approaches to direct-reading spectroscopy which successfully circumvent some of the problems connected with direct-current integration systems have been devised. Early investigations on mechanical-scanning, gated, pulse integration techniques for direct-reading spectroscopy by Brehm and Fassel (2) and Bullock and Silverman (3) have illustrated the advantages of a rapid, spectral-scanning method. The term pulse integration indicates that signal pulses which correspond to spectral lines were integrated instead of a direct-current signal. These integrations correspond to current-time integrals for each pulse over many pulses and should not be confused with the pulse counting methods used in x-ray spectrometry. A gated amplifier is one that electronically is switched "on" and "off" by a square wave voltage pulse. This pulse is applied to the grid of an amplifier tube that is normally biased to "cut off". Upon application of the gating pulse, the vacuum tube conducts

and acts as a typical electronic amplifier during the interval which corresponds to the width of the pulse. Typically, in such an arrangement, the dispersed radiation is intercepted by a plane mirror or mirrored prism which is rotated by a synchronous motor. Brehm and Fassel (2) used a plane mirror which was located before a 1.5 meter Wadsworth camera such that spectral lines were focused on the plane of an adjustable slit directly in front of the cathode of an end-on photomultiplier. Background corrections were automatic and independent of direct current drift, and slit alignment and shift were no longer significant problems. However, these aspects are overshadowed somewhat by the complexity of the mechanical features of the rapid scanning device and electronic circuits associated with the separation of the signals which result from individual spectral lines. In general, this type of instrument has not been widely used.

Benn et al. (4), Agnew et al. (5) and Andreev (6) have employed image orthicon and iconoscope tubes as spectroscopic detectors. Their experimental arrangements involved placement of one of these storage-type camera tubes so that a spectrum was focused on the planar photosensitive surface. The signal was then presented on an oscilloscope screen which had its

horizontal scanning beam synchronized with the electron beam of the camera tube. Andreev (6) has reported successful integrations of the iconoscope output signal, but detailed information on circuitry and results is lacking. Although these types of detectors have a wide range of spectral response and eliminate the problems associated with the exit slits, they do not exhibit the linear response over orders of magnitude of input radiant flux that is characteristic of common vacuum photomultipliers. Also, the significant lack of uniformity of the image orthicon photocathode surfaee has subjugated this detector to semiquantitative measurements only.

Another conceivable approach to direct-reading spectroscopy centers on the image-dissector, multiplier phototube. This phototube has a magnetically-focused electron lens system and an aperture between the photocathode and the first dynode of the secondary electron multiplication system. Effectively, this opening interposes a spatial limit on the photocathode area viewed by the first dynode of the tube. The electron image, which is a reproduction of an optical image on the photocathode, is focused upon the aperture plane and deflected in a regular, periodic fashion by a magnetic field from an external coil. For spectroscopic applications,

the optical and electron images are, naturally, those of spectral lines which are defined at the focal plane of a spectrograph. Upon synchronizing a sawtooth current through the deflection coil with the horizontal, sawtooth voltage sweep of an oscilloscope, a display of vertical voltage pulses which correspond in magnitude and position to the relative intensity and position of each spectral line focused upon the photosensitive surface of this end-on phototube can be observed. The principal characteristics of such a device feature non-mechanical scanning ability along with the near-instantaneous and wide-range linear response of the common vacuum photomultiplier. These tubes then can, in principle, provide the following distinctive advantages over the classical direct-reading schemes:

a. Spectrograph exit slits and their associated positioning problems are eliminated.

b. Background signal corrections are not necessary, for the pulse-area integration method enables blockage of the direct-current background signal. Direct currents from other electronic sources can be blocked by ac coupling.

c. The capability to do gated integrations alleviates the problem of "slit isolation" of a single spectral line which is close to one or more other lines in the focal plane of a spectrograph.

A retrospective consideration of the unique characteristics and capabilities of the image dissector multiplier phototube prompted this investigation of its potential and applicability as a detector in direct-reading spectroscopy.

II. HISTORICAL AND PRELIMINARY DISCUSSION

A. History of Direct-Reading Techniques

The first direct-reading instrument, which was constructed by Lundegårdh in 1934 (7, p. 104), consisted of a photocell attached at the exit slit of a monochromator. An amplified signal from the photocell deflected a galvanometer, and the degree of deflection was directly related to relative spectral line intensity. Later attempts to improve upon this design (8, 9, 10) met with little practical success because of the instability and lack of sensitivity characteristic of the photoelectric detectors available at that time.

Demands on the steel industry during the early phases of World War II brought a renewed interest in photoelectric spectral analysis because of the need for precision analyses that would not consume the time and manpower required by the classical chemical methods. Fortuitously, this interest was concurrent with the introduction of the first commercial phototubes that employed secondary-emission multiplication of photocathode current. Application of photomultipliers to the direct determination of spectral line intensities by scanning the spectrum over a single exit slit and measuring the

continuous photocurrent developed alongside and contributed to the growth and refinement of direct-reading methods (11).

In 1942, Applied Research Laboratories of Glendale, California initiated commercial development and production of direct-reading instrumentation in this country (12) with a direct-reading spectrograph which came to be known as the "Quantometer". Hasler was among the early few to recognize the capabilities (12) and economic significance (13) of the direct-reading spectrograph for the steel industries. Advantages gained by this electronic read-out system over spectrographic techniques primarily are attributable to the inate characteristics of the photographic emulsion. Although the photographic technique is of great value in cases where a large number of lines from a fluctuating light source must be recorded simultaneously, photoelectric measurements are easier and much faster to make. Coheur and Hans (14) have estimated direct-reading analysis time to be 60 seconds plus 5 seconds for each additional element and approximated spectrographic analysis time to be 5 minutes plus 20 seconds for each additional element. Both of these estimates assume fully operative conditions for each method. Analyses for as many as 67 elements can be performed simultaneously with

present-day instrumentation (15). Since photoelectric intensity-ratios as large as 10^5 to 1 can be measured conveniently, and photographic intensity ratios are restricted to values considerably less than 10^2 to 1 (16), whole ranges of high-percentage analyses, not so readily performed by spectrographic methods, can be accomplished by the direct-reading method (17). Accuracy comparable to chemical methods can be obtained, and precision is better than that attained spectrographically (17). Coefficients of variation for analysis in the range 0.6 to 0.8 percent have been reported by Coheur and Hans (14).

The versatility of the direct-reading spectroscopic technique in analysis of a wide range of sample types is well documented in the literature. Numerous papers on quality control in steel and metal production methods (18-30), application to agricultural problems (31) and review articles on applications (32-37) and instrumentation (38-44) have been published within the last two decades.

B. Electronic Signal Measurements

The difficulties and restrictions on accurate, electronic measurements of low-intensity light signals encompass all the problems generally encountered in the determination of very

small electrical signals. Indefinite amplification of a small signal will not necessarily improve the ability to measure voltage, for the always-present noise will be increased by the same factor. The term noise refers to any current or voltage which is extraneous to and interferes with the signal of interest. Since noise power is additive (45, pp. 251-252), the magnitude of noise signal at an amplifier output is a direct function of the spurious signals and bandwidths contributed by the signal source, detector and all amplifier components.

A noise contribution can be categorized in terms of its origin as either spurious or fundamental. The former class of noise sources is typified by (a) distortion of a signal by the amplifier (amplitude, phase, harmonic or intermodulation), (b) electromagnetic pickup (ground loops, etc.), (c) magnetic fields, (d) power supply fluctuations, (e) hum, (f) microphonics and (g) partition noise which is due to random fluctuations in the division of signal current between two or more electrodes in a multigrid, vacuum tube. The influence of these noise sources can be minimized through careful design considerations. Fundamental noise refers to random fluctuations from thermal and shot effect origins, and represents

the ever-present, lower limits of noise that must be tolerated for any electronic measurement system.

Thermal noise is due to the random motion of free electrons in conductors and has been treated theoretically in the Nyquist equation (46, p. 193):

$$\bar{E}_{rms} = (4RkT\Delta f)^{\frac{1}{2}},$$

where $\bar{E}_{rms}$ = root-mean-square noise voltage, R = resistance of the element in ohms, k = Boltzmann constant (1.38×10^{-23} joule/degree), T = absolute temperature ($^{\circ}K$), and Δf = bandwidth of the circuit in Hertz. The practical implications of this equation are threefold: (a) amplifier bandwidth should be reduced to a minimum without distorting the signal of interest, (b) circuit temperature should be kept as low as possible, and (c) R should be low in critical circuits. In the latter instance, only the input resistor value is considered, for the noise from this resistance is amplified more than the noise generated at later stages of amplification. Also, special low-noise resistors are available for use in critical locations.

Shot noise results from a current passage in vacuum tubes and transistors that consists of a transfer of

discrete charges. The random fluctuations in the total current at the plate or collector originate from this transference of unit charges. Schottky (47) has developed an equation which describes the maximum shot-effect noise:

$$\bar{E}_{rms} = (2qIR_L^2\Delta f)^{\frac{1}{2}},$$

where $\bar{E}_{rms}$ = root-mean-square noise voltage, q = charge on each carrier in coulombs, I = total current through tube in amperes, R_L = load resistance value in ohms, and Δf = bandwidth in Hertz. This expression suggests use of narrow bandwidth, a small load resistance and small currents through a vacuum tube. Generally, for vacuum tubes, $\bar{E}_{rms}$ is smaller than the calculated value because of an averaging effect by space charges in the tubes.

Another type of noise of uncertain origin occurs only when a direct current is present in a conducting element and is commonly known as "1/f" noise or current noise. Since experimental observations of this noise have shown that it is greatest at low frequencies and increases with the square of the direct current, an empirical relationship between the root-mean-square voltage noise ($\bar{E}_{rms}$), current (I) and frequency (f) has been suggested (48, pp. 270-271):

$$\bar{E}_{rms} = KI^2/f,$$

where K is an empirical constant derived from the type of resistance material and geometry of the resistor. This type of noise is generally high in composition resistors and can be much greater than thermal noise up to frequencies of 10^3 Hz (48).

The figure of merit which customarily is chosen to describe the purity of a signal waveform is the signal-to-noise ratio (S/N). Usually, this value is given as a power ratio in decibels; S/N(db power) = 10 log $\frac{\text{signal power}}{\text{noise power}}$, or a voltage ratio in decibels; S/N(db voltage) = 20 log $\frac{\text{signal voltage}}{\text{noise voltage}}$.

C. Photomultipliers as Detectors in Direct-Reading Spectroscopy

Just as the basic character of spectrographic analysis is reflected by the properties of photographic emulsions, the fundamental nature of photoelectric methods is dependent largely on the attributes of photomultipliers.

A typical photomultiplier possesses a layer of photoemissive material which is deposited on the inner surface of a window segment of an evacuated glass envelope.

Photoelectrons which emanate from this cathodic surface are collected by a tube element known as a dynode. The electrons from the photocathode are accelerated by a potential difference between the photocathode and first dynode, and collide with the dynode surface to produce a number of electrons greater than that quantity collected from the photosurface. This process is referred to as secondary-emission multiplication and is commonly employed repeatedly to increase photoelectron currents to levels that are convenient to measure. The number of dynodes that can be incorporated in a multiplier system usually is limited by considerations of electron optics and geometry. Total gain of the tube depends on the dynode surface material, acceleration potentials and the number of dynodes. Typically, the current gain at each dynode stage is about three.

The general qualities of strict linear response, high gain with low noise, stability, short response time, long life and the conveniences afforded by electrical measurements were recognized in early developmental stages of the photomultiplier (16, 49-53). However, dark current, noise and gain stability of photomultipliers became much more critical

factors in electronic measurements as the radiation flux densities to be measured became very small.

The response of a photomultiplier to spectral radiation is dependent on the composition of the photocathode material (54). Commercial photocathodes are categorized by standard spectral response numbers, and responses of several of the more common types are illustrated in Figure 1. Each surface has a different thermal work function (55) and accordingly, presents a different dark current under equivalent sets of conditions. Dark current is measured at the anode of the photomultiplier with no radiation incident on the cathode and is thus a function of gain, cathode area and cathode composition. In general, surfaces, such as the S-1 type (Ag-O-Cs), which respond to red radiation, exhibit dark currents that are much greater than those for the S-11 or S-20 response types. However, the S-20 surface (Sb-K-Na-Cs: multialkali) which has much better red response and higher quantum efficiency than the S-11 type (Sb-Cs on Mn-MnO layer), has a thermionic emission level that is equal to (56) or lower than (54) that of the S-11.

Just as a knowledge of prominent sources of noise in amplifier systems is requisite to the attainment of accurate

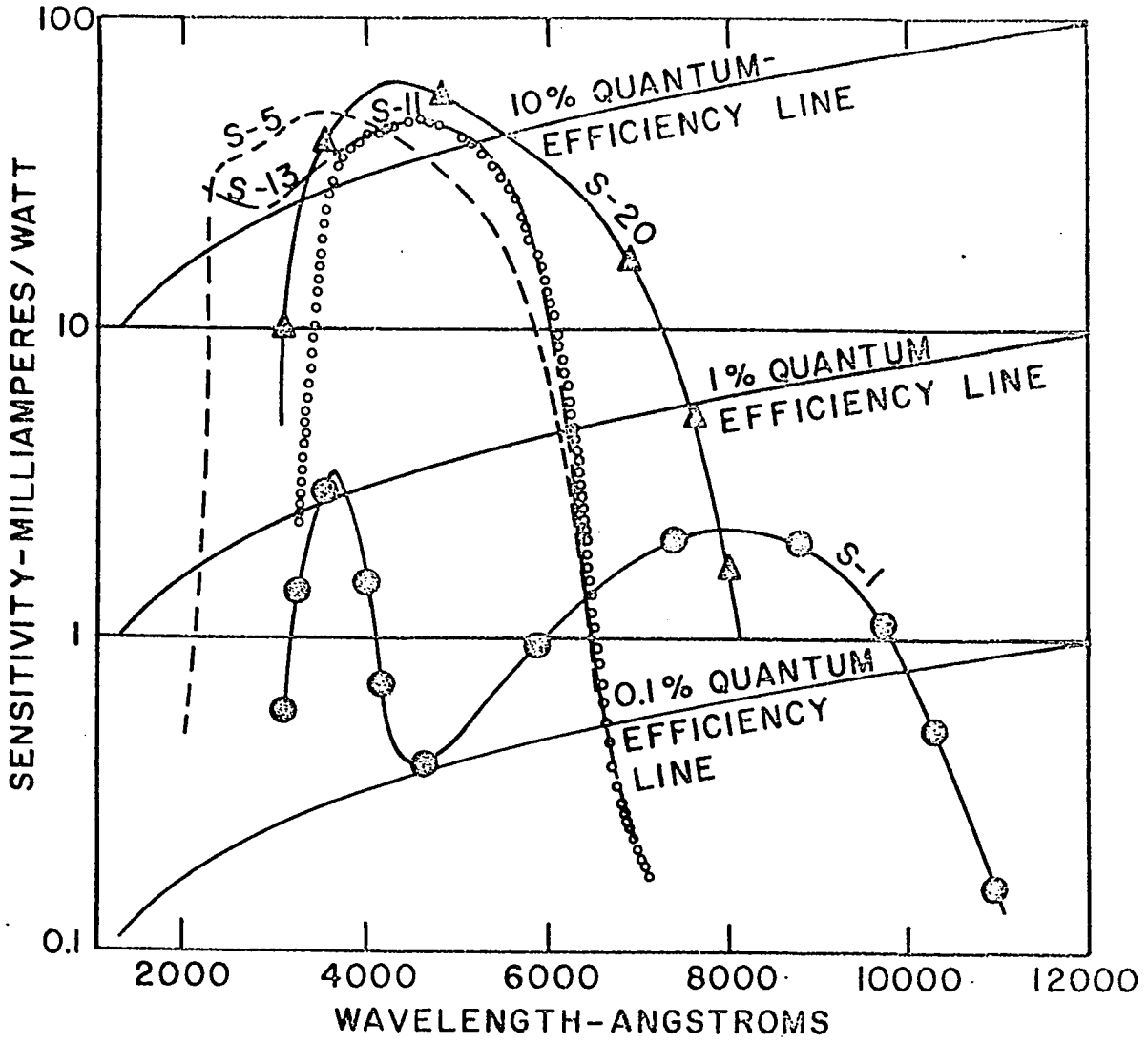

Figure 1. Spectral response curves of some common photosurfaces

information, a familiarity with the character and magnitude of noise from the detector employed is a necessity.

Again, two general classifications of noise exist. Spurious noise can originate in the power supply as leakage currents, or as field emission, or from ion feedback in the photomultiplier tube. Fundamental noise is produced in thermionic emission from the photocathode, as shot-effect noise in the signal current and as current fluctuation due to the secondary emission process. Noise originating from fluctuations in the signal flux will not be considered here.

For photomultipliers which are operated at room temperature, threshold sensitivity is limited by the thermal electrons which are emitted from the photocathode. The threshold sensitivity is the lowest level signal that can be detected at the photocathode, and this threshold is assumed to be reached when the radiant power incident on the photocathode produces a peak signal current which equals the root-mean-square fluctuation current from all sources at the photocathode. This threshold condition is defined by the radiant power quantity, which is the equivalent noise input, and the dark current contribution to total signal noise power, which can be calculated from the photocathode

sensitivity, dark current and bandpass (57):

$$\text{Dark Current Noise in Signal ENI} = \frac{(2ei_D\Delta f)^{\frac{1}{2}}}{S_k \times 10^3},$$

where ENI = equivalent noise input in watts, e = electron charge in coulombs, Δf = bandwidth in Hertz, S_k = cathode radiant sensitivity in mA/watt, and i_D = dark current in amperes at cathode.

Obviously, since dark current diminishes with a decrease in temperature a simple method to improve threshold sensitivity for surfaces with low thermal work functions is to cool the photoemissive layer. The thermal electrons from the photocathode produce a current density at the cathode which depends on temperature and can be approximated by the Richardson equation (58):

$$j_k = BT^2 e^{-E/kT},$$

where j_k = current density at cathode in A/cm^2, B = constant with the units $A\ (cm^2\ T^2)^{-1}$, T = absolute temperature (°K), E = thermal work function in joules, and k = Boltzmann constant (1.38×10^{-23} joule/degree). Most of the practical photosurfaces are not pure metals but combinations of two or more metals or compounds. These complex surfaces have multiple work function characteristics which cause large

deviations from Richardson's law at low temperatures (55). Generally, thermionic emission can be predicted accurately near room temperature (273-323°K) provided values for B and E are known. Eberhardt (59) has reported that the dark current noise for the FW-118 photomultiplier, which has S-1 response, diminishes about an order of magnitude for every 20°K temperature decrease, and dark current is reduced by a factor of 10 for each 10°K temperature decrease. That such an approach to reduce dark current is commonly attempted appears well documented in the publication of many photomultiplier cryostat designs (49, 60-69) and applications to spectroscopic studies (16, 70-75) and astronomy (76, 77). Also, dark current and effective noise have been reduced for some types of photomultipliers through use of photocathode surfaces with small areas.

The second important source of noise incurred with a photomultiplier is shot noise. This fluctuation in signal current occurs only when a light flux impinges on the photosurface, and its contribution to the total signal noise at the anode can be approximated mathematically from the cathode sensitivity and bandpass (57):

$$\text{Shot Noise in Signal ENI} = \frac{2\ e\ \Delta f}{S_k \times 10^3},$$

where ENI = equivalent noise input in watts, e = electron charge in coulombs, Δf = bandwidth in Hertz, and S_k = radiant sensitivity in mA/watt.

The quality of construction and design of the multiplier phototube are generally left to the manufacturer and electronics specialists. However, once an experimentalist purchases a photomultiplier, the performance and function of the tube are largely determined by the individual who plans to use the phototube. Special attention should be given to attainment of recommended dynode potentials before construction of the voltage divider bridge. Signal-to-noise ratio properties of the electron multiplication system are principally dependent on the collection efficiency of the first two dynodes, and thus, focus conditions are very important (78). This fact contains the real virtue of photomultipliers, for the total reduction of signal-to-noise ratio which is attributable to the multiplier is not dependent on the number of dynodes. Normally, a photomultiplier should not be exposed to bright room light just before use, for phosphorescence of tube components can contribute to the dark current signal. In order to prevent irreparable damage to a photomultiplier, the photosurface should be exposed to low

light fluxes only, and high anode currents should be avoided. However, even if the light fluxes and currents of concern are somewhat more moderate, severe fatigue effects may be observed. Fatigue refers to a time dependent variation in sensitivity or gain. Sometimes, the term hysteresis is used to indicate a short duration change, and fatigue is reserved to mean long time-interval changes. Kaye (79) has ascribed hysteresis effects to variations in electron transfer efficiency that are produced by electrostatic charges on the insulators supporting the dynodes. The position of the illuminated region on the cathode appears to be the factor which has the greatest influence on hysteresis. Fatigue arises from changes in the secondary emission ratio that result from volatilization of cesium from the dynode surfaces. Unlike hysteresis, the fatigue process is cumulative. Usually, a photomultiplier which has noticeable hysteresis and fatigue effects should be stabilized by prior exposure of the photosurface to radiation of a frequency and flux density similar to the light intensity to be measured.

Refrigeration of a photomultiplier in order to reduce dark current and thermal noise compounds stability problems. The phototube must be cooled slowly to avoid breaking the

glass envelope, and once a desirable temperature level has been attained, this temperature must be maintained to prevent anode current drift. Water condensation on the base pins can produce leakage currents and noise, and frost formation on the tube or cryostat-housing window can attenuate the signal produced by incident radiation.

D. The Magnetically Focused Image-Dissector, Multiplier Phototube

Philo T. Farnsworth introduced the image-dissector, multiplier phototube as the first successful means for television by electron image scanning in 1930 (80-94). Before this time, image dissector tubes without secondary electron multiplication had proven to be unsatisfactory, for luminous fluxes of 15 to 25 lumens were required to produce a signal impulse above the noise level. Upon the introduction of a secondary electron multiplier system into the structure and behind the internal aperture of the tube, current amplifications greater than 10^3 with no significant increase in noise were attained. Such an improvement made possible the use of this camera tube under more moderate illumination conditions.

Zworykin and Morton (95) have traced the development of the image dissector photomultiplier as a camera tube for television.

The operation of the image dissector phototube is based upon the conversion of an optical image into an electron image. An optical image, sharply focused upon a uniform photoelectric surface (photocathode), produces an electron emission which is proportional to the luminous intensity incident at each point. This photoelectron pattern at the cathode plane is termed the electron image of the optical scene. Spectral response extends over all regions for which photocathodes are available. This implies that regions from the near infrared to the extreme ultraviolet are accessible.

A uniform magnetic field, axially oriented with respect to the cylindrical phototube envelope, provides a focus of the electron image upon a planar, anode target which is parallel to the cathode surface and contains a small aperture. The random velocities (in the vector sense) of the emitted electrons result in interactions with the magnetic field which cause the electrons to follow helical trajectories into the target plane. Of course, those electrons emitted in a direction perpendicular to the cathode plane do not interact

with the magnetic field. Proper adjustment of the field strength via the focus coil current and of the anode target potential gives a one-to-one correspondence between the electron "picture elements" on the cathode and those on the anode.

This electron image can be deflected with another electromagnetic field. A suitable sweep mode is provided by a sawtooth waveform current drive of the concentrically mounted deflection coil. Such a periodic waveform provides a relatively slow, linear change in position of the electron image which is then terminated and followed by a rapid swing back to an initial image position on the anode. This magnetic deflection accomplishes a motion of the electron image across the aperture of the target anode. Thus, through the period of motion of this image, a continuous presentation of image intensity information is given to the first dynode in the secondary electron multiplication structure as an electron beam in elementary portions defined by the size and shape of the aperture. For each unidirectional sweep of the electron image, the intensity distribution, as defined by the anode aperture, along the sweep direction axis can be displayed on an oscilloscope screen. If the output signal from the last

dynode of the electron multiplier dynode chain is employed for vertical deflection of the cathode ray tube beam and the magnetic sweep function synchronized with the horizontal oscilloscope sweep, a readily interpreted signal display is obtained. Either magnetic or electric deflection can be used, however the former method has proven to be more readily adaptable to low voltage transistor drive circuitry.

In the role as a scanning detector, the image dissector possesses some rather unique properties. Unlike the orthicon or vidicon camera tubes, the image dissector multiplier phototube is a non-storage tube. Thus, an instantaneous signal character is obtained instead of the time-integrated signals scanned by these storage tubes. The rapid scan can be stopped to permit use of the image dissector as a conventional photomultiplier detector which provides an unmodulated output signal. On-axis resolution attained is closely predictable on the basis of a selected aperture size that defines the electron beam. Off-axis resolution approaches that of on-axis only for the magnetically focused tubes. The secondary electron multiplier principle pertinent to image dissectors provides for linear response over at least four to five orders of magnitude in the range of normal usage. A greater

dynamic range can be accommodated by readjustment of the multiplier gain through an alteration of the applied operating potential. Since the image dissector phototube does not have a thermionic cathode, such as the orthicon and vidicon tubes possess, it consumes less operating power and functions for a longer period of time.

Noise can normally be attributed to three readily identified origins: photocathode dark emission, background lighting on the photocathode, and the signal flux. Nearly all photocathodes, except those which are infrared sensitive, have extremely low dark emission noise. Thus, the image-dissector phototube generally can be expected to operate either under a background noise limited or noise-in-signal limited condition.

The only reported spectroscopic application of the image-dissector, multiplier phototube was revealed recently by Harber and Sonnek (96). This publication disclosed the use of an S-11 response image dissector on a low dispersion (131 Å/mm), Czerny-Turner spectrograph. The apparatus was constructed for the study of sources of intense, transitory radiation phenomena, and made scans over a spectral range of 2500 Å at rates of 100 or 1000 scans per second. Resolution obtained with an internal, 51 μ by 5.1 mm, slit-shaped

aperture was related to be 10 Å. Only oscilloscope traces of the rapid spectral scans were utilized, and no attempt to perform signal integrations for careful quantitative analyses was mentioned.

III. EXPERIMENTAL

A. The Image-Dissector Photomultiplier and Pulse-Integration System

1. Selection of an image-dissector photomultiplier

The carbon-arc extraction technique for the determination of oxygen and nitrogen in steel (97, 98) represents a typical situation in which the high dark current characteristic of S-1 response photomultipliers limits the sensitivity and precision of analysis. The most intense arc emission lines are relatively weak and occur in the 7700 to 8200 Å region. Thus, upon integrating photocurrents with the conventional dc apparatus, very much uncertainty in the integrated line intensity exists because this intensity represents the difference between two large, uncertain integral values. Since there is presently no other known photosurface that is so responsive to radiation in this portion of the spectrum, the status quo must either be accepted or another approach to the problem must be sought.

The other approach to this specific problem and similar ones is embodied in the application of an S-1 response, image-dissector photomultiplier. Such a detector is capable

of providing the required response to red radiation without the undesirable background signal. Since this one very significant advantage of the image dissector is best illustrated by a red-sensitive photocathode, an S-1 cathode was chosen for the image dissector employed in this investigation.

Detailed characteristics of the type F-4011 image-dissector photomultiplier (International Telephone and Telegraph Industrial Laboratories, Fort Wayne, Indiana) which was utilized in this study, are given in Table 1. A schematic of the image dissector appears in Figure 2. The NJE regulated, photomultiplier power supply described later provided a constant 1300 V for the image dissector voltage divider bridge.

2. A housing for the image dissector

In order to mount the image dissector onto the 0.5 meter Ebert spectrometer, whose optical properties are described in a later section, the exit slit and accompanying slit mounting plate were removed from the spectrometer. The slit mounting plate, which was an aluminum plate of solid construction built to rigidly support entrance and exit slits, was cut into two portions, and the half that normally maintains the entrance slit in position at the collimating mirror focus was attached to the spectrometer in the firm, original position.

Table 1. Description of the F-4011 image dissector multiplier phototube

Feature	Specifications
Response type	S-1
Diameter (in)	1.5
Length (in)	8.2
Photocathode diameter (in)	1.1
Cathode luminous sensitivity (μA/L)	20
Typical current amplification (at 2000 V)	5×10^4
Approximate cathode-to-aperture target voltage (V)	600
Internal aperture dimensions (mm)	0.05 x 4.29

A special housing for the image dissector, 15-VF-349-X focus coil and 15-VY-301, 1.5 inch vidicon deflection yoke (International Telephone and Telegraph Industrial Laboratories, Fort Wayne, Indiana) was designed and constructed. A scale drawing of the housing is presented in Figure 3. This housing also accommodated the voltage divider bridge, electrostatic focus potentiometer and provisions for independent, precise

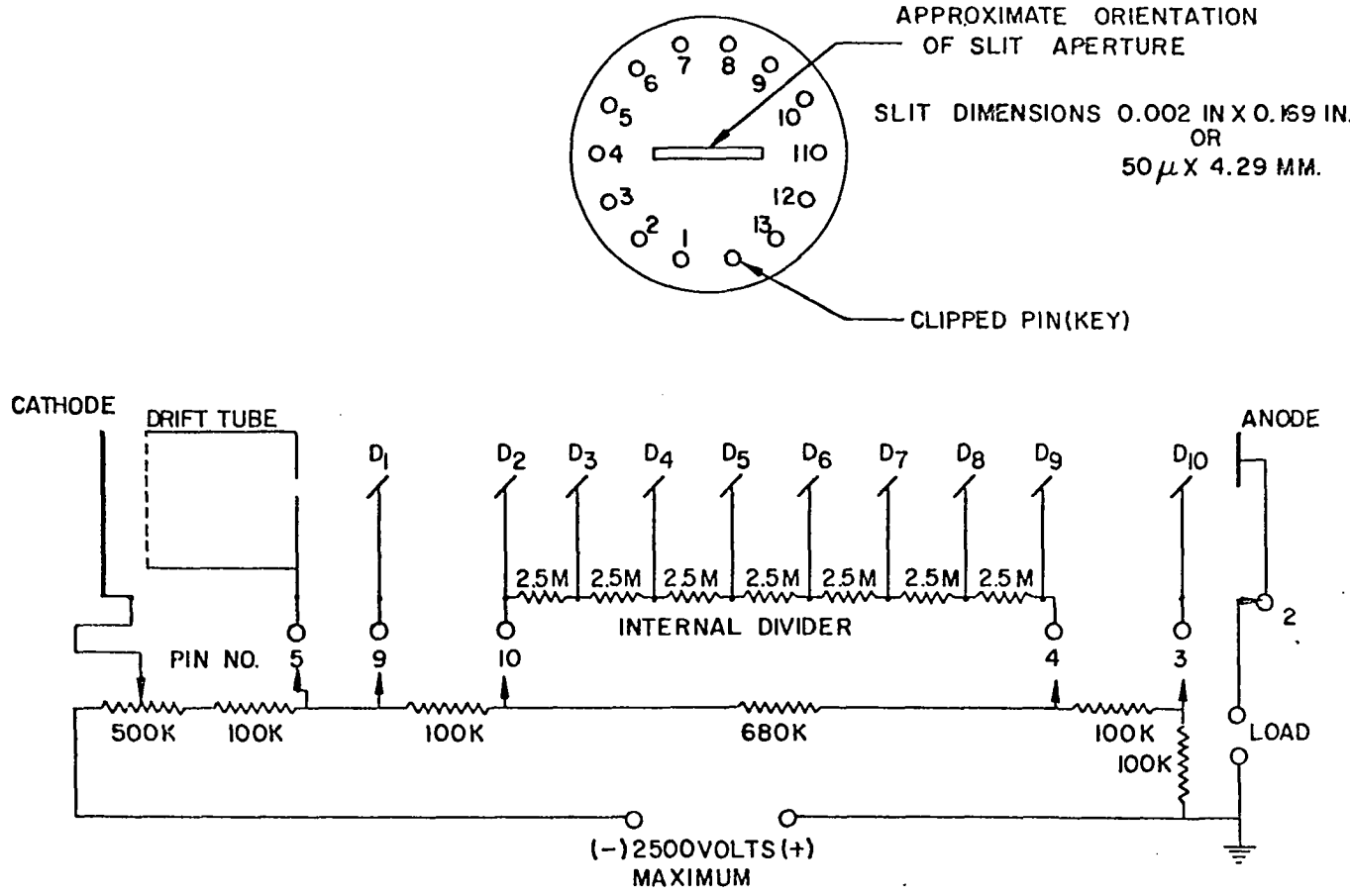

Figure 2. Schematic of F-4011 image-dissector, multiplier phototube

Figure 3. Scale drawing of housing for F-4011 image-dissector, multiplier phototube

A. Aluminum base
B. Clamp on rotational adjustment
C. Aluminum rotational adjustment with one-degree marks over a fifteen-degree interval
D. Rotatable brass base
E. BNC connectors (Amphenol Co.) to high-voltage input and signal output
F. Ground connection to solder lug
G. Potentiometer (screw-driver adjustment) for electrostatic focus adjustment
H. Screw which clamps aluminum, split-ring, stop to rotatable brass base
I. "Unislide" screw assembly (Tropel, Inc., Fairport, New York) for fine optical-focus adjustment (40 turns/inch)
J. "Bakelite" encasement for all external resistors in the voltage divider bridge
K. Electrical lead to cathode
L. Pin base connector for photomultiplier
M. ITTIL F4011-S-1 image dissector photomultiplier
N. Cylindrical brass housing
O. Aluminum clamp for "Unislide" screw attachment
P. Focus and deflection coils
Q. Electrical leads to focus and deflection coils
R. Brass mounting bracket to attach housing to spectrometer
S. Aperture of spectrometer

END VIEW

CUT-AWAY SIDE VIEW

SCALE
1 INCH

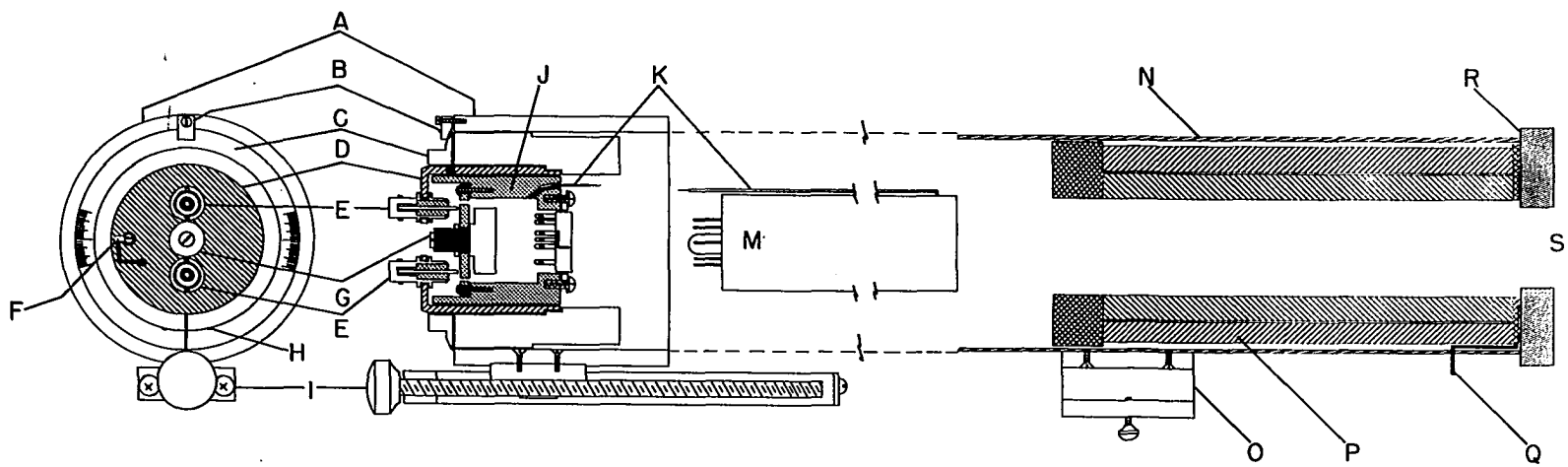

optical focus and rotation adjustments. The curvature of the 0.5 meter Ebert focal plane necessitated a fine, optical focus adjustment, and rotation of the image dissector was required to align the slit-shaped, internal aperture with the spectral lines defined by the 25 μ entrance slit. A photograph of this housing on the 0.5 meter Ebert spectrometer is presented in Figure 4.

3. Focus and sweep coil current supplies

The focus of electrons from the photocathode surface of the image dissector upon the internal aperture was accomplished through control of the direct current supplied to the focus coil. Constant currents in the 15 to 40 mA range were provided for the focus coil by the supply shown in Figure 5. Mr. Dale W. Hilker of the Ames Laboratory Electronics Shop designed and constructed this circuit. A repeated current waveform through the deflection coil moved the electron image across the internal slit in a well-defined periodic manner. The sawtooth current function (the particular waveform used is sometimes referred to as a ramp) for the sweep coil was provided by the supply shown in Figure 6. The circuitry was designed by Mr. Dean Van Zuuk and constructed by Mr. Raymond C. Prior, both of whom are associates of the Ames Laboratory

Figure 4. Photograph of image dissector housing on 0.5 meter Ebert spectrometer

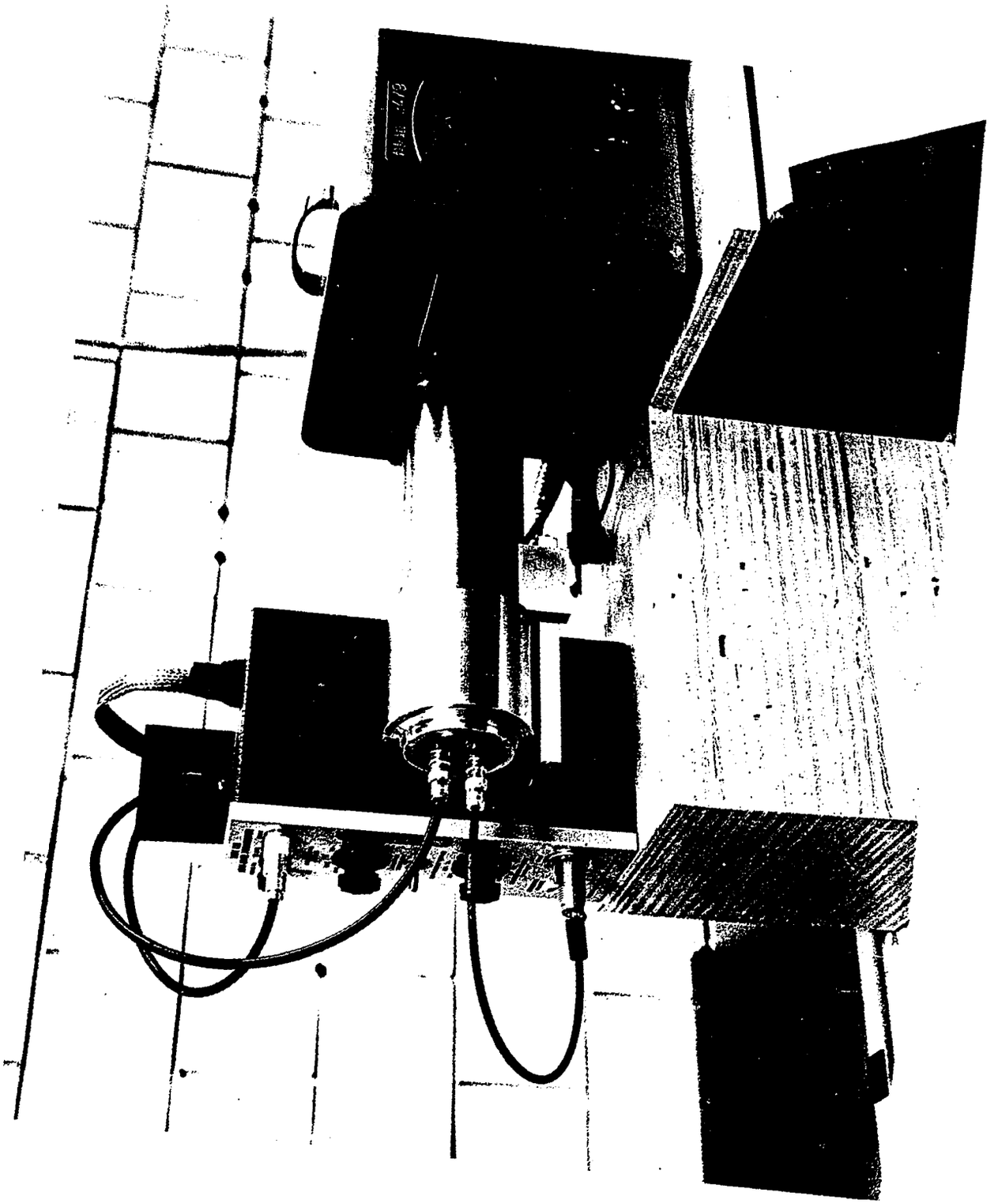

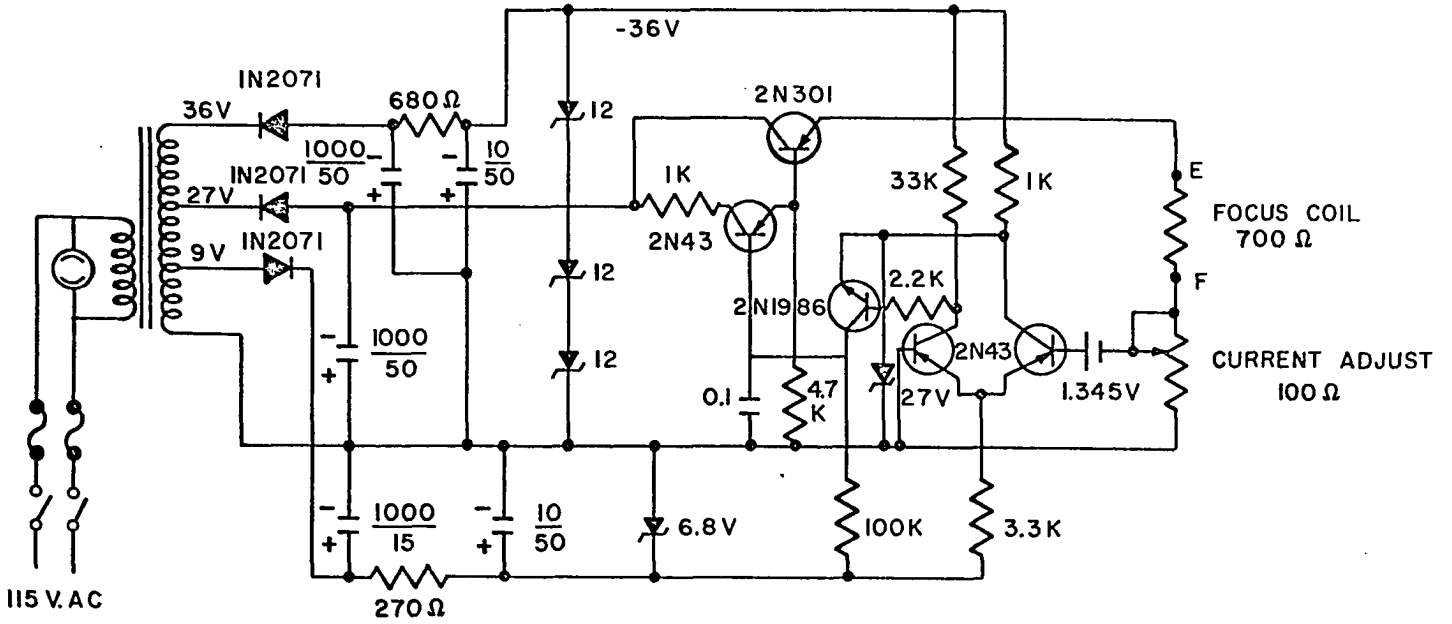

Figure 5. Current supply for focus coil

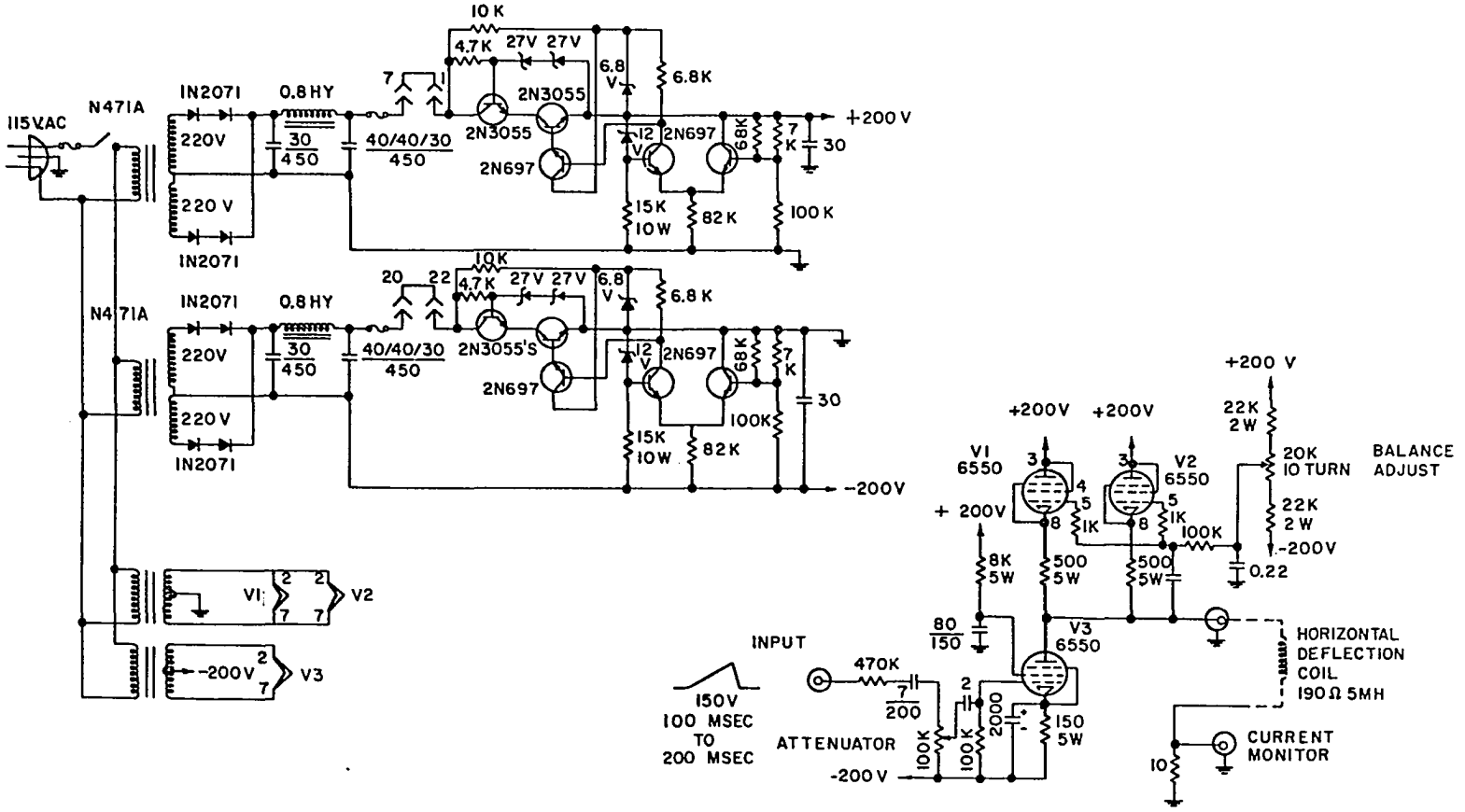

Figure 6. Sweep supply for deflection coil

Electronics Shop. Sweep currents in the range 60 to 170 mA were utilized, and good linearity proved to be in the 100 to 200 msec per sweep time interval (10 to 20 msec/cm on the cathode ray tube graticule). A 150 volt sawtooth signal from either time-base of a Tektronix oscilloscope (type 545A, Tektronix, Inc., Beaverton, Oregon) provided activation of the current sweep supply. This arrangement made possible a conveniently variable sweep frequency that was readily synchronized with the cathode ray tube display.

4. Preamplification of the signal from the image-dissector anode

The output signal from the image dissector first was fed to a Tektronix type 122 preamplifier (Tektronix, Inc., Beaverton, Oregon). This ac-coupled, three-stage amplifier increased the voltage signal by a factor of approximately 100. All operating voltages to this amplifier, including the filament supply, were from batteries. The bandpass, which could be selected by front-panel switches, was set for the 0.8 to 250 hertz, "3-db points". General characteristics of this amplifier are presented in Table 2.

Table 2. Characteristics of the Tektronix type 122 preamplifier

Feature	Specification
Operating modes	Single ended or differential
Input impedance	Single ended: 10M paralleled by 50pF Differential: 20M paralleled by 50pF
Output impedance	About 1K from a cathode follower
Gain	Either 100 or 1000
Maximum ac input level (peak-to-peak)	0.02 V at high gain 0.10 V at low gain
Input stage noise level	Less than 15 μV (peak-to-peak)
Amplifier linearity	Within 5%

5. Signal display and pulse-integration systems

The sawtooth current supply to the deflection coil repeatedly sweeps the electron image of a selected spectral region past the internal aperture of the image dissector as described in detail above. A display of these preamplified signal pulses resulting from each scan may now be presented on a cathode ray tube, or integrated over a set time period or for a given number of sweeps. The oscilloscope display of three close spectral lines would appear much as the pulses sketched in part 1 of Figure 7.

A display of the spectrum is essential to spectral line identification, but further "processing" of the pulses which represent a single spectral line must be performed for a successful integration. That is, the pulse which corresponds to the spectral line of interest must be, in a step-wise manner, isolated from other line pulses, integrated and stored.

The isolation of a line pulse can be accomplished by gating the amplifier to which the preamplified signal produced by the image dissector is continuously supplied. That is, a gating signal (2 of Figure 7), which is synchronized with the pulse signal of interest, electronically turns "on" this amplifier every sweep cycle. During the "on" interval, which

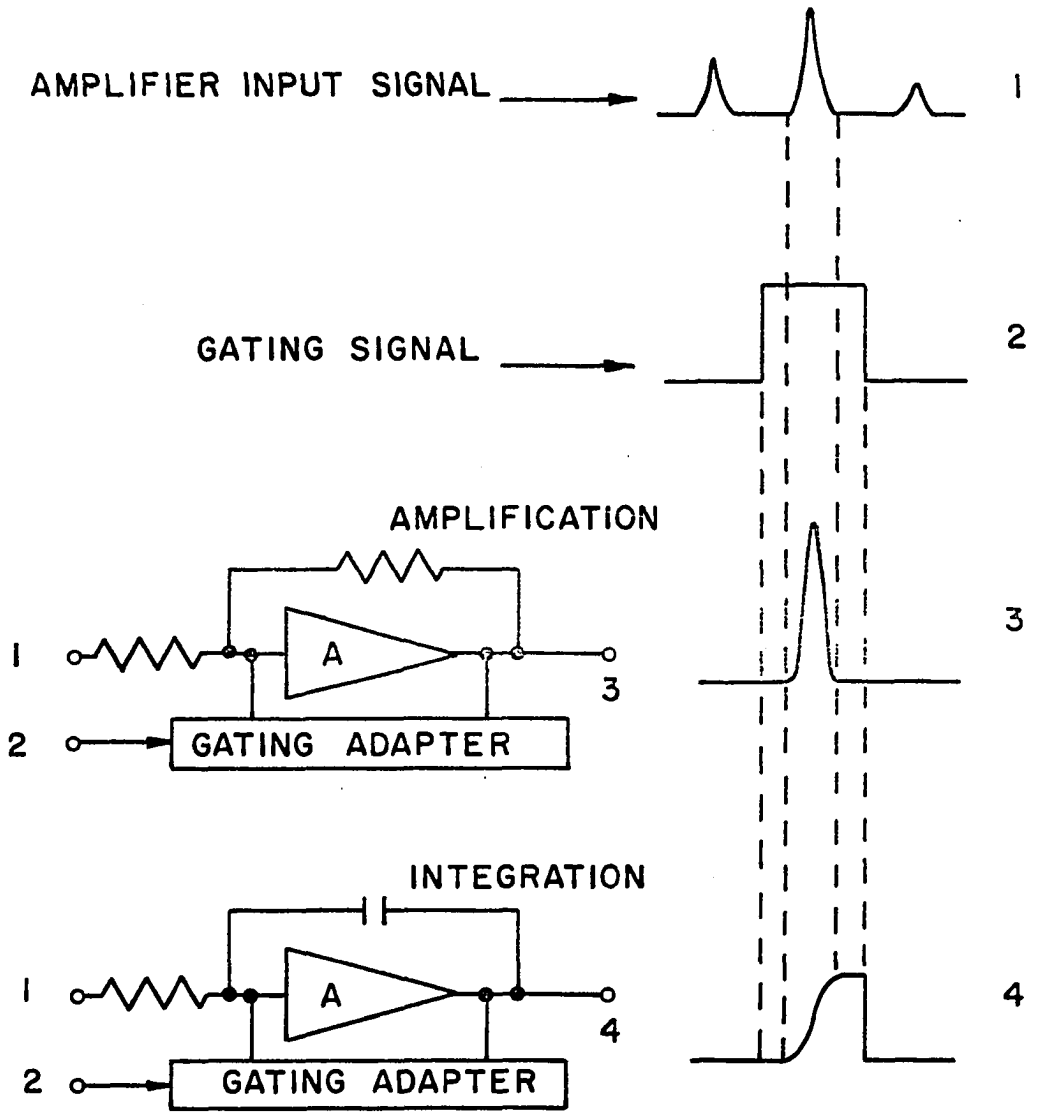

Figure 7. Illustration of signal synchronization in a gated-integration or gated-amplification system

corresponds to the width of the gate pulse in time, the amplifier performs some function on the isolated pulse. At all other times, the amplifier is "off". If this amplifier were an operational amplifier, the function might be simple amplification (3 of Figure 7) or integration (4 of Figure 7). Without such an isolation of single line pulses, the operation chosen would be performed on all pulses occurring in each sweep.

In the system employed for this investigation, which is shown in Figure 8, isolation of voltage pulses originating from a spectral line was achieved with the operational amplifier gating control and gated operational amplifier of a Tektronix oscilloscope. The Tektronix type 545A oscilloscope (Tektronix, Inc., Beaverton, Oregon) proved to be a versatile and convenient center around which the associated equipment was designed and built. This oscilloscope derives its versatility from a dual time-base and a variety of plug-in module amplifiers. One of the plug-in units, the Tektronix type "O", was employed to perform a gated amplification of the spectral line signal pulses from the preamplifier. This plug-in consisted of two operational amplifiers and an additional adapter circuit which enabled the performance of gated

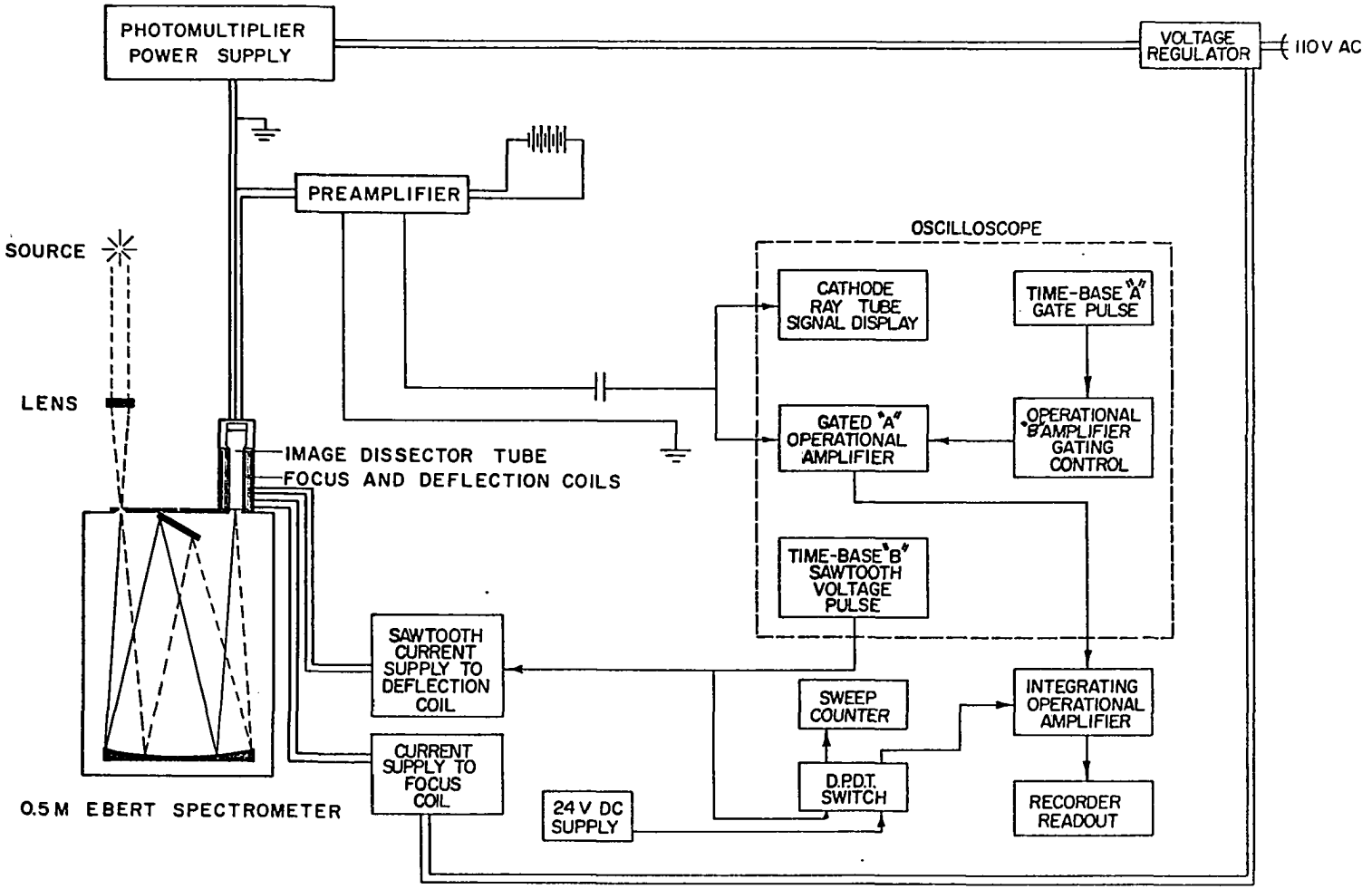

Figure 8. Image-dissector direct-reading system

amplifications or gated integrations. The two operational amplifiers in the plug-in module were designated "A" and "B" by the Tektronix Company. Referring now to Figure 8, one can follow the path of the preamplified signal from the image dissector through a 0.29 μF shielded, coupling capacitor to the inputs of the oscilloscope vertical amplifier and the "A" operational amplifier. The "B" operational amplifier was modified by the addition of a Tektronix, plug-in gating adapter (Figure 9). Thus, the "B" operational amplifier, which received a gate pulse from the oscilloscope "A" time-base, was used to precisely gate "on" and gate "off" the "A" operational amplifier. The "A" amplifier remained "on" for the duration of the 20 volt, square-wave gating pulse, and was "off" during the time between gating pulses.

The mechanism through which the gating adapter and "B" amplifier functioned to control the "A" amplifier can be elucidated by a careful consideration of Figure 9. Repetitive positive gate pulses having the form shown in part 2 of Figure 7 produced a voltage drop across the Zener diode (1N753, Figure 9) and maintained a charge on the input capacitor. The input pulses were negatively offset after passing through the diode-capacitor network because of

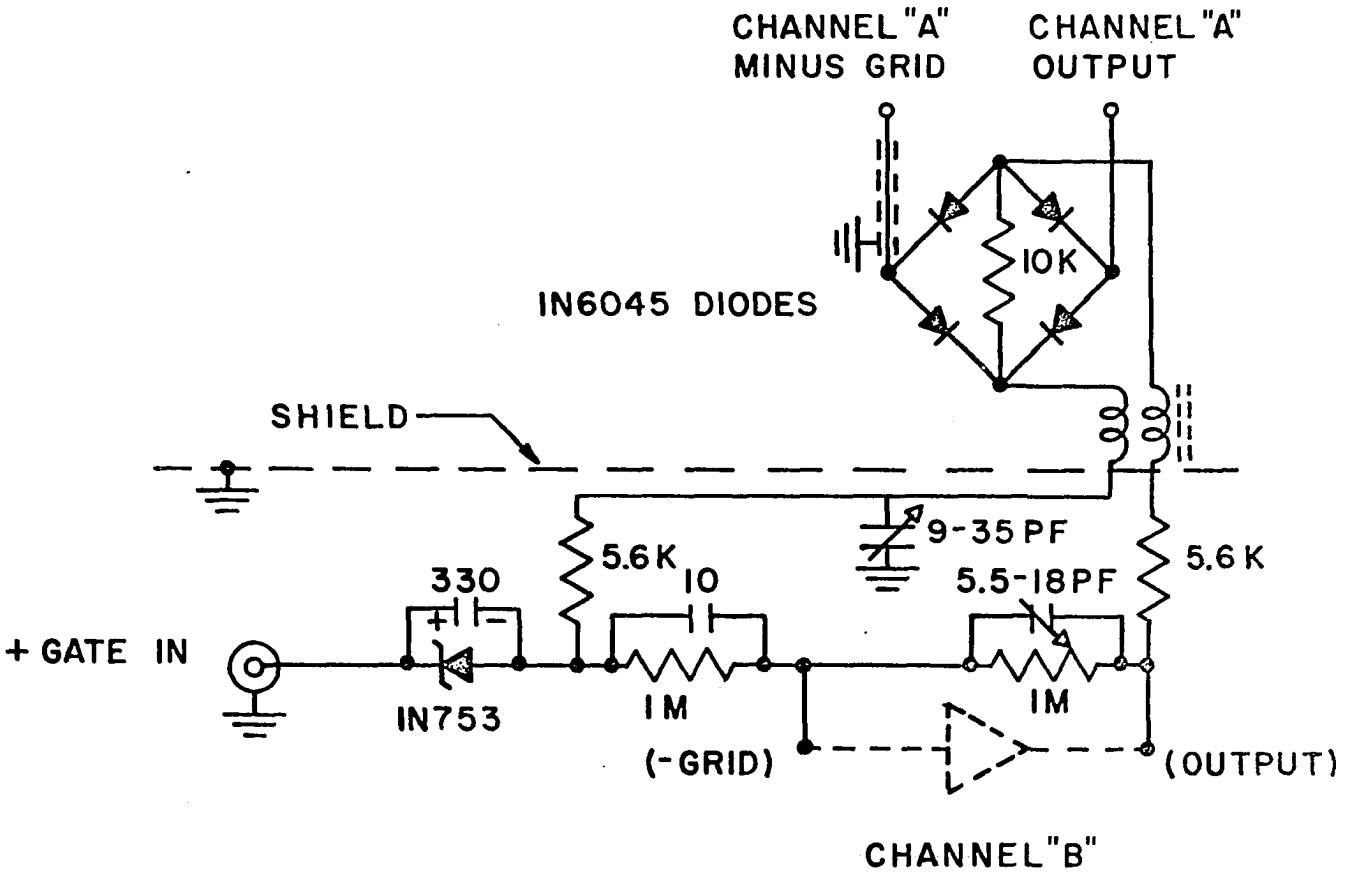

Figure 9. Tektronix gating adapter

this charge. The "B" operational amplifier was connected simply as a unity-gain, inverting amplifier that applied equal-amplitude, reversed-polarity pulses across the diode bridge. During a gating pulse interval, all four diodes were back-biased and demonstrated a resistance of about 2×10^{11} ohms in parallel with the "A" amplifier feedback impedance. Since such a high parallel resistance did not alter significantly the feedback impedance value, the "A" amplifier was turned "on". At the end of a gating pulse, the stored charge on the input capacitor reversed the polarity of the voltage across the diode bridge. Then, all four diodes conducted and appeared as a low resistance in parallel with the feedback impedance of amplifier "A". Upon this reduction of feedback impedance to nearly zero ohms, essentially no signal appeared at the "A" output and the "A" amplifier was "off". The characteristics of the two identically constructed, Tektronix operational amplifiers are given in Table 3. The oscilloscope vertical amplifier, which was also part of the type "O" plug-in unit, had a 14 nsec risetime and a bandpass from dc to 25 MHz. Nine calibrated vertical-deflection factors were provided at 0.05, 0.1, 0.2, 0.5, 1, 2, 5, 10 and 20 volts per centimeter. Continuous adjustment from 0.05 to 50 volts per

Table 3. Specifications for Tektronix operational amplifiers

Feature	Specification	Comment
Open loop dc gain	2500	Gain of the amplifier without external feedback.
Gain-bandwidth product	15 MHz	Frequency at which the gain has "rolled off" to unity.
Gain roll-off	6 db/octave	Rate at which the open-loop gain falls off with increasing signal frequency.
Drift	Less than 10 mV per hour (referred to input)	Change of offset voltage with time.
Input noise (wideband)	0.5 mV (peak-to-peak)	Normalized value of any output disturbance not contained in the input signal.
Input impedance	Selected by front-panel control: 0.01, 0.1, 0.2, 0.5 and 1 megohm; 10 pF, 0.0001, 0.001, 0.01, 0.1 and 1 μF.	

Table 3 (continued)

Feature	Specification	Comment
Output impedance	30 ohms at 1 MHz for compensated unity-gain amplifier.	
Feedback	Positive or negative.	
Grid current	Less than 0.5 nA.	
Output range	±50 V, ± 5 mA.	
Output dc level	Ground potential (adjustable)	
Error factor in gain	Compensated to unity for all internal impedances.	

centimeter was facilitated by a variable, uncalibrated control. Input impedance of the amplifier was approximately 1 megohm paralleled by 47 pF.

The gain factor of the gated "A" amplifier usually was set at about 2. Gate time-widths generally were about ten percent of the oscilloscope sweep interval. Proper time-coherency between the gate pulse and the input line signal was attained through use of the oscilloscope time-delay circuitry. This synchronization of gate and signal pulses could be observed on the oscilloscope display. Start of the horizontal, oscilloscope sweep could be delayed from 1 μsec to 10 sec after the application of the triggering waveform. This delay was accomplished through simultaneous use of time-base "A" and time-base "B". The term time-base refers to an independent, trigger-multivibrator, Miller sweep-circuit system. The "B" time-base provided accurate time delay while the "A" time-base presented a normal horizontal sweep at the end of the delay interval. Selection of continuously variable delay times was possible in the utilized operating mode. Thus, time-width of the gate "on" interval for the gated operational amplifier was set by adjusting the "A" time-base sweep interval to a value equal to about 10 percent of the "B" time-base sweep interval

("A" delayed by "B" mode). Then, the gate position (position of the "A" sweep with respect to the "B" sweep) was adjusted by varying the time-delay interval.

At this stage, the spectral line pulse has been displayed on the oscilloscope so that it could be identified and electronically separated from pulses produced by other spectral lines. The tasks of integrating many of these isolated line pulses, storing the charge on a capacitor and measuring the resulting voltage remains.

This final process of integration and storage was performed by the integrating operational amplifier indicated in Figure 8. A Philbrick, chopper-stabilized, operational amplifier (model USA 3, G. A. Philbrick Researchers, Inc., see p. 361 of reference 46 for the schematic) enabled this last signal transformation. The accumulated charge on the feedback capacitor (2 μF $\pm$ 5%, 100 V dc, teflon dielectric, Southern Electronics, Burbank, Cal.) of this amplifier increased with every sweep over the isolated spectral line of interest. The accumulated voltage on the capacitor was continuously recorded with a high-impedance strip-chart recorder (model FWD, Texas Instruments, Inc.). This recorder was specified to have a 0.5 sec time constant and 2 to 4 megohm input impedance.

The full-scale span of the recorder was 10 mV. Since the linear charge range of the integrating capacitor was stipulated to extend to 50 mV, integration linearity was assured.

However, this recorded voltage on the feedback capacitor was not meaningful as an integral until it could be associated with a number of sweeps across the image-dissector internal aperture required to produce the measured voltage. A 7-digit capacity pulse counter (model 7360R, Universal EPUT and Timer, Berkeley Scientific Division of Beckman Instruments, Inc., Richmond, California) was used for counting sweeps.

At this stage of signal "processing", means have been established to produce a voltage pulse which corresponds to a spectral line of interest, isolate this pulse from others, integrate the pulse, store the voltage integral and continuously read out this integral voltage on a recorder as the sweeps which produce spectral line pulses from the image dissector are counted. For practical purposes, there remained the one problem of beginning and ending the integration process while simultaneously starting and stopping the sweep counter. This was achieved with the simple double-pole, double-throw switch illustrated in Figure 8. One side of the switch conducted the 150 volt sawtooth sweep signal from the oscilloscope "B"

time-base, which had been modified through an addition of a simple cathode-follower amplifier circuit in order to drive the sweep coil supply. The other side of the switch carried a 24 volt, dc signal to activate a relay which was internal to the Philbrick operational amplifier plug-in module and thereby start the integration process.

In practice, the integrations were performed in one of two ways: either the number of sweeps required to accumulate a definite voltage was counted or the integrated voltage for a measured number of sweeps was determined. These later integral voltages could then be adjusted to a self-consistent scale for the purpose of plotting analytical calibration curves because the magnitude of the recorded integral voltage was directly proportional to the number of sweeps required to produce it.

Two subsidiary pieces of electronic equipment heretofore undescribed must be mentioned to make this description complete. The first of these units involves the high voltage sources for the operational amplifier responsible for signal integrations. Voltages of +300 V and -300 V for the Philbrick amplifier were obtained through a dropping resistor from the

oscilloscope +350 V supply and an extra B+ supply, respectively. The latter voltage supply unit also provided a high-current capacity 6.3 V for the amplifier filament circuit and was specified to have a long-term drift variation less than 0.01 percent per hour.

All electronic units in the total, direct-reading system which did not have self-contained voltage regulation were connected to a 2 KVA, ac voltage regulator (model 1750, Sorenson and Company, Incorporated, Stamford, Connecticut).

A photograph of the image-dissector direct-reading system is illustrated in Figure 10. The spectrometer, optical system and preamplifier were resting on the chasis of a Perkin-Elmer model 13, infrared spectrometer unit and a massive plywood-block shelf in this photograph.

6. General operating procedure for pulse integrations

After a one hour warm-up period for all electronic components, the zero offset controls on the Philbrick and Tektronix operational amplifiers were adjusted in a preliminary manner so that no output signal (integral) appeared over the desired integration period. With the premixed, oxy-acetylene flame (described later) operating and nebulizing a solution of the analyte elements, the grating of the spectrometer was

Figure 10. Photograph of image-dissector, direct-reading system

rotated until spectral lines of interest were located in the oscilloscope display. Then, the width and position of the gate were set with the time-delay controls on the oscilloscope face panel to isolate the desired spectral line pulse. With the flame source running but nebulizing only absolute ethanol, the offset controls were readjusted to eliminate any output signal that originated from background band structure. Generally, flame background in the red of the spectrum was found to be low for all zones of the flame, and thus such a correction of zero offset was not necessary. Signal integrations were then performed by activating the integration circuit and sweep counter.

Up to this point in the discussion of the image-dissector direct-reading system, the reader has been expected to accept the fact that true integrations of voltage waveforms can be accomplished with electronic devices that have been referred to as operational amplifiers. Rather than continue without some explanation, several of the general capabilities and specific properties of these amplifiers which reflect the qualities and limitations of a system in which they are employed are now considered.

The capability of an electronic circuit to perform a mathematical integration of a voltage waveform is not a property that is intuitively obvious. In order to provide some insight into the means by which this type of integration can be performed, an analysis of the instantaneous voltage across a capacitor in the simple "RC" circuit of Figure 11 is detailed below.

For purposes of illustration, let the input voltage, E_i, be a sinusoidal wave-form:

$$E_i = E_p \sin \omega t, \qquad [1]$$

where E_p = amplitude or peak voltage, ω = angular frequency, and t = time. At low frequencies, the instantaneous current, I, through this circuit is out-of-phase with the voltage and leads the voltage by the phase angle φ.

$$I = I_p \sin (\omega+\varphi) t, \qquad [2]$$

where I_p = amplitude or peak current. The charge, Q, on the capacitor, at any time is related to the capacitance value, C, and voltage, E_c.

$$Q = CE_c . \qquad [3]$$

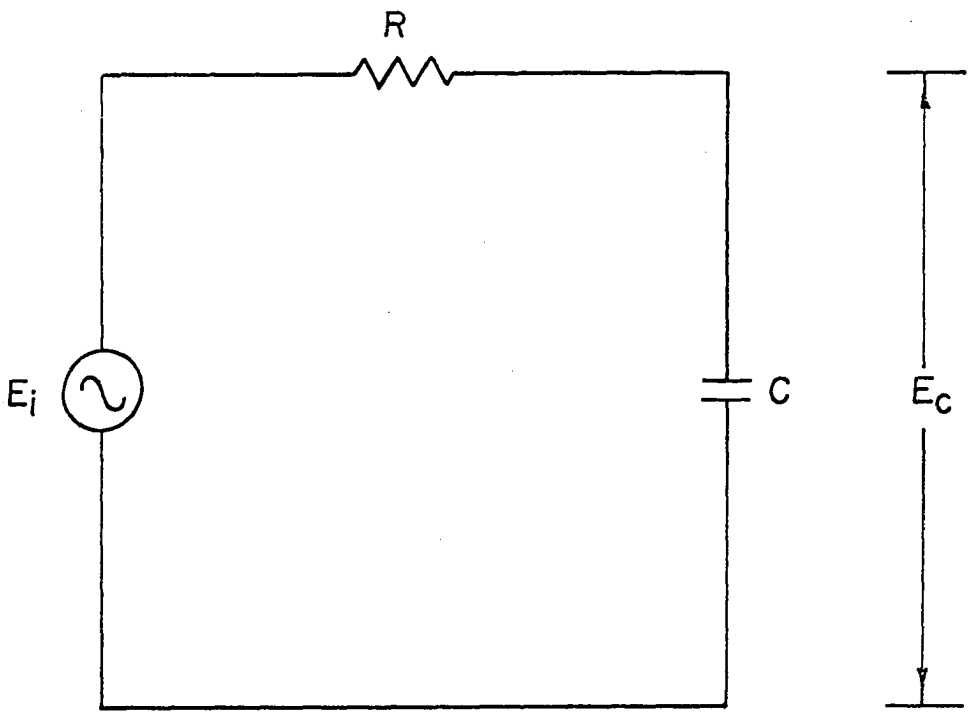

Figure 11. A simple "RC" circuit

The derivative of equation [3] with respect to time is

$$\frac{dQ}{dt} = C \frac{dE_c}{dt} \quad . \qquad [4]$$

By the definition of current,

$$I = \frac{dQ}{dt} \quad . \qquad [5]$$

Thus, $$I = C \frac{dE_c}{dt} \quad . \qquad [6]$$

$$dE_c = \frac{1}{C} I dt. \qquad [7]$$

$$E_c = \frac{1}{C} \int I dt. \qquad [8]$$

Substituting for I in equation [8] with the expression from equation [2] provides that

$$E_c = \frac{1}{C} \int I_p \sin (\omega + \varphi) t \, dt. \qquad [9]$$

If $R >> X_c$, where X_c is the capacitative reactance in the circuit, the following approximations are true:

$$\varphi = 0, \; Z = R, \qquad [10]$$

where Z is the impedance of the circuit. Then, equation [9] is simplified, and

$$E_c = \frac{1}{C}\int I_p \sin \omega t \, dt . \qquad [11]$$

Since $E_i = IZ$, [12]

and $Z = R$, then

$$E_p = I_p R . \qquad [13]$$

If I_p from equation [13] is substituted into equation [11],

$$E_c = \frac{1}{C}\int \frac{E_p}{R} \sin \omega t \, dt. \qquad [14]$$

$$E_c = \frac{E_p}{RC}\int \sin \omega t \, dt \qquad [15]$$

$$E_c = -\frac{E_p}{\omega RC} \cos \omega t', \qquad [16]$$

where t' = time interval.

From equation [16], $E_c = \frac{1}{RC}\left[-\frac{E_p}{\omega} \cos \omega t'\right]$. [17]

Then, considering the integral of E_i from equation [1],

$$\int E_i dt = \int E_p \sin \omega t \, dt. \qquad [18]$$

$$\int E_i dt = -\frac{E_p}{\omega} \cos \omega t'. \qquad [19]$$

A comparison of equations [17] and [19] shows that

$$E_c = \frac{1}{RC}\int E_i dt. \qquad [20]$$

Therefore, for the circuit of Figure 11, the instantaneous voltage across the capacitor is equal to the product of the reciprocal of the "RC" time constant and the time-integral of the input voltage.

Since a simple case of the electronic integration of a voltage waveform now has been elucidated, let us consider the operational amplifier as an integrator. Operational amplifiers obtained their name from an early application as a high quality, dc amplifier which could perform mathematical operations in analog computers. These amplifiers are characterized by stability, high gain and large, negative, voltage feedback. Negative feedback results from a 180° phase shift between the input voltage signal and the amplified output signal. A high input impedance minimizes the loading of any source, and low output impedance enables the amplifier to drive almost any load. Although dc coupling to the signal source is typical, the amplifier will respond to signal frequencies which range from 10^5 hertz to dc. Figure 12 illustrates the operating modes of immediate concern. The schematic symbol for a phase-inverting amplifier with gain A is the triangle shown in the figure. Z_i and Z_f are external feedback impedances. Gain (G) of the closed-loop amplifier is given by

A. OPEN-LOOP OPERATION

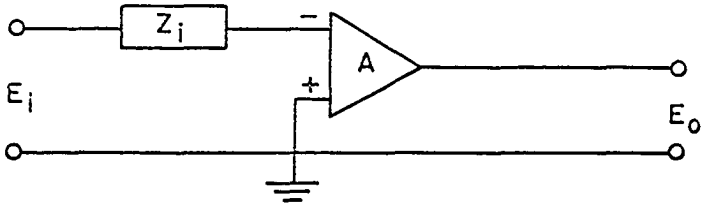

B. CLOSED-LOOP OPERATION FOR NEGATIVE FEEDBACK

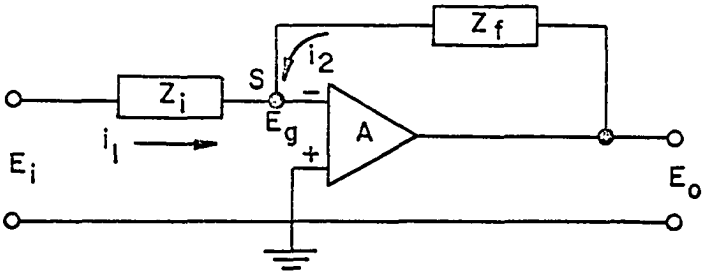

$$i_1 + i_2 = 0 \text{ AT S.}$$

$$E_o = E_g A$$

C. INTEGRATING CIRCUIT

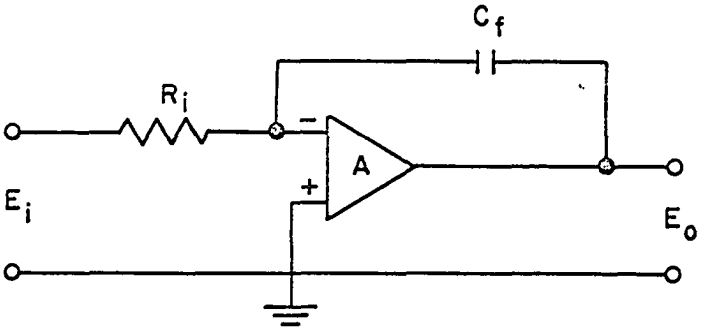

Figure 12. General operation modes of concern for operational amplifiers

the expression

$$G = \frac{E_o}{E_i} = - \frac{Z_f}{Z_i} \left[\frac{1}{1 - \frac{1}{A} (1 + \frac{Z_f}{Z_i})} \right].$$

The term in brackets is referred to as the error factor, because it reflects a dependence of gain on more than a simple impedance ratio. The minus sign on the gain expression symbollizes the phase shift of the output voltage. Amplifier gain decreases with increasing signal frequency, and the effect is generally compensated in the multistage amplifier to produce a smooth roll-off of 6 db per octave. This prevents oscillation by the amplifier at any value of closed-loop gain.

For the integration circuit (Figure 12, C), the current (i_1) through external resistance R_i equals E_i/R_i. Assuming that grid current is negligible, current i_1 charges the feedback capacitor C_f. Output of the amplifier is essentially the voltage across the capacitor because of the virtual ground at the grid of the amplifier (point S in Figure 12, B). The voltage across the capacitor (C_f) and thus, the output voltage is

$$E_o = -\frac{1}{C_f}\int i_1 dt.$$

Since $i_1 = -\frac{E_i}{R_i}$,

$$E_o = -\frac{1}{R_i C_f}\int E_i dt.$$

Therefore, output voltage of the amplifier is proportional to the integral of the input voltage.

High frequency components in a waveform tend to be eliminated by integration. This is the result of the inverse proportionality between output voltage of the integrator and frequency of the input. An illustration of such frequency dependence is given in the following example. For a sinusoidal input waveform $E_i = E \sin \omega t$, where E = peak amplitude, ω = angular frequency and t = time,

$$E_o = -\frac{1}{R_i C_f}\int E \sin \omega t \, dt.$$

Thus, $E_o = \frac{-E}{R_i C_f \omega}(-\cos \omega t)$. Additionally, phase shift of the output signal is shown by this expression. Gain (G) of the integrator circuit which is the ratio of the amplitudes, is also frequency dependent: $G = \frac{E_o}{E_i} = -\frac{1}{R_i C_f \omega}$.

Even with very careful design and well-stabilized supply voltages, drifts in dc amplifiers are difficult to prevent. Drift voltages at the amplifier output indicate that operational feedback no longer keeps the branch point (S) at virtual ground. This error in virtual ground is called offset. Offset voltages tend to change with temperature and time, and typically are about 10 mV. A constant offset voltage results in an ever-increasing output signal for an integrating circuit. Without proper balance of the offset voltage and good stability, integration of small voltages over long periods of time is not possible. Two other errors arise in integrating circuits. Current leakage to the summing point (S) from nearby power supply leads or other sources are integrated and confused with the signal current. This problem can be avoided by proper shielding of the summing-point wiring. Capacitor leakage produces error current and an unstable integral. High quality integrating capacitors must be employed to eliminate such an effect.

7. Use of the image dissector as a conventional dc detector

The ability of direct-reading spectroscopic systems to provide high reproducibility in photoelectric measurements represents one of the generally accepted attributes of this

analytical technique. A comparison between the measurement precision of the image-dissector operated both as a direct-reading and conventional dc detector in spectral-scanning was possible in this particular instance. In a spectral-scanning system the dc output from a photomultiplier is recorded continuously as a spectrum is slowly scanned past the single, spectrometer exit slit. This scan is accomplished by rotating the grating with a constant speed, synchronous motor. In order to obtain this precision data for conventional operation, the image dissector was used with only the magnetic focus field and the high voltage supplied to the voltage divider bridge.

Output signal from the image dissector was fed directly into the input of a Keithley model 417, high-speed picoammeter (Keithley Instruments). This amplifier used an electrometer tube input with solid-state amplifiers and power supply. Specified input impedance ranged from 100 ohms at the 10^{-5} A, full-scale setting to 10^{4} megohms at the 10^{-13} A, full scale setting and changed in decade steps with the scale setting. There were eighteen current ranges from 10^{-13} to 3×10^{-5} A full scale. Accuracy was stipulated to be $\pm 2\%$ of full scale from 3×10^{-5} to 10^{-8} A, and $\pm 3\%$ of full scale on

other ranges. Zero drift was specified to be less than 1% per eight hours. The manufacturer's estimate of the rise time in the range employed was 4 msec. Output from this Keithley amplifier was fed to the Texas Instrument, model WFD recorder which is described later. This arrangement permitted the recording of emission source, relative intensity versus wavelength.

B. Auxiliary Equipment

1. Spectroscopic sources

A flame and a hollow cathode lamp were chosen as spectroscopic sources for this investigation because of their stability and the absence, during operation, of strong, fluctuating magnetic fields, such as those generated by spark-type discharges, which could interfere with the oscilloscope trigger circuits.

A Re hollow cathode lamp with Ne filler gas (Type WL 22942, Westinghouse Electric Corporation, Electronic Tube Division, Elmira, New York) was utilized in initial alignment adjustments and stability investigations. The regulated current supply for the hollow cathode lamp provided direct

currents below 20 mA that showed long term variations of less than 0.05 percent.

A premixed, oxy-acetylene flame was employed to provide line spectra of the common alkali metals. Solutions of the alkali metal chlorides in absolute ethanol were used throughout this investigation. The burner and flame, with the zones typical to very fuel-rich operation, are illustrated in Figure 13. Generally, gas flow rates were such that the interconal zone was very small. A 5 mm high portion of the region above the primary reaction zone was viewed by the spectrometer for most observations.

2. Gas pressure-flow regulation for flame source

Since the intensities of line and background spectra from the flame were very dependent on the combustion mixture, a precise, monitoring system was employed to maintain these variables within narrow limits over the data collection intervals. The pressure-flow monitor system utilized has been described in detail in an earlier publication (99).

3. External optics

A spherical quartz lens (4.4 cm diameter, 25 cm focal length) was mounted between the flame and spectrometer. The lens focused an unmagnified, inverted flame-image on the

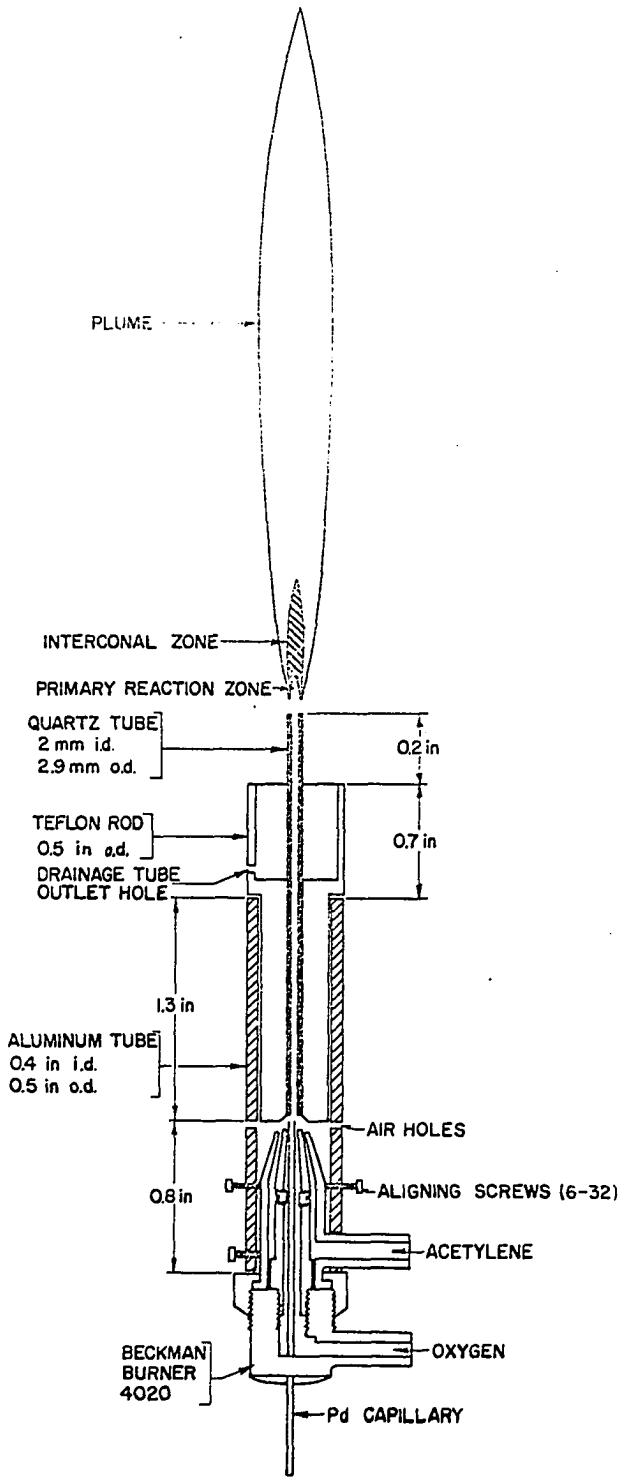

Figure 13. Premixed, oxy-acetylene flame and burner

entrance slit.

High order spectral interference was reduced through use of a sharp "cut-off" filter (CS3-67, Corning Glass Works, Bulletin CF-1). The filter "cuts-off" radiation below 5400 Å.

4. Spectrometer

A Jarrell-Ash, 0.5 meter, Ebert spectrometer, with the characteristics summarized in Table 4, served as the dispersing device. Spectral scan speeds of 10 Å/min and 125 Å/min were used for quantitative line peak-height measurements and wide-range, strip chart traces, respectively.

C. Experimental Facilities for Evaluating S-1 Response Photomultipliers in dc Operation Modes

1. Photomultipliers

In section II-C, a detailed discussion of the effects of photocathode areas and temperature on the dark currents of S-1 response photomultipliers was presented. Either cooling the photocathode or effectively limiting the cathode area produce a diminished dark current and lower noise. Thus, just as with the image dissector, there are other direct means to drastically reduce the large dark currents typical of these S-1 response tubes and, in this sense, improve the

Table 4. Description of Jarrell-Ash model 82000 Ebert scanning spectrometer

Feature	Specifications
Optical arrangement	Ebert grating mount. 500 mm focal length mirror. Effective aperture ratio f/8.6.
Grating	Plane reflection, 1180 grooves/mm over a 52 x 52 mm ruled area, on a blank 58 mm square. Blazed for 7500 Å.
Dispersion	16 Å/mm reciprocal linear dispersion in first order.
Slits	Fixed, bayonetting, 16 x 0.025 mm entrance and exit slits were used for investigations with conventional photomultipliers. A 16 x 0.025 mm entrance slit was used with the image dissector.
Scanning action	Manual and automatic scanning modes were available. Automatic scan speeds of 500, 250, 125, 50, 20, 10, 5 and 2 Å/min were at hand.

capabilities to measure weak line intensities in the near infrared. Since the investigator has these two other means (or a combination of the two) to reduce the contribution of dark current to the total observed signal, a comparison of the capabilities of each approach was of great interest.

For these comparison studies, two photomultipliers of very different construction were chosen. The characteristics of the FW-118 (International Telephone and Telegraph Industrial Laboratories, Fort Wayne, Indiana) and C70007A (Radio Corporation of America, Harrison, New Jersey) S-1 response, head-on type photomultipliers selected for use as detectors throughout the direct current integration studies, are detailed in Table 5. The effects of the differences in cathode areas and possible current amplification on other properties of each photomultiplier should be noted and kept in mind.

The FW-118 photomultiplier had an electrostatically focused electron lens system with a 0.200 inch by 0.200 inch (5 x 5 mm) defining aperture in the electron image plane and between the first dynode and photocathode to limit the effective photocathode area. The purpose of the feature was to reduce equivalent noise input by minimizing collected thermionic emission current and ion feedback while

Table 5. Description of photomultipliers

Feature	FW-118	C70007A
Effective cathode area (mm^2)	25 (Planar cathode)	1420 (approximate) (Spherical cathode)
Number of dynodes	16	12
Typical anode dark current at 25°C (A)	3×10^{-6}	1.2×10^{-6}
Spectral response type	S-1	S-1
Average cathode photo-sensitivity ($\mu A/L$)	20	20
Typical equivalent noise input (Watts)	2.7×10^{-13}	1.7×10^{-12}
Typical current amplification	10^7 at 1800 V	7.5×10^5 at 1250 V

simultaneously maintaining a high photoelectron collection efficiency in the effective photocathode area.

The C70007A photomultiplier utilized a focusing electrode with external connection for shaping the field which directs photoelectrons from the cathode onto the first dynode. A spherical photocathode surface assured that the first dynode would collect electrons from all parts of the useful photocathode area.

2. Cryostat housing for photomultipliers

Since the performance of these S-1 response photomultipliers was expected to improve at low temperatures, provisions to refrigerate both photomultipliers were made. The Andonian photomultiplier, cryostat housing (Andonian Associates, Incorporated, Waltham, Massachusetts) is illustrated in Figure 14. Cooling of the inner chamber of the housing was accomplished by throttling liquid nitrogen through a helical, metal coil which was in contact with the high-conductivity, metallic cylinder that defined the inner walls of the cryostat. Surrounding, thermal insulation was provided by in situ styrofoam insulation. The inner chamber was continuously flushed with dry helium gas (50 to 100 ml/min flow), and the outer side of the evacuated, double-wall quartz window was

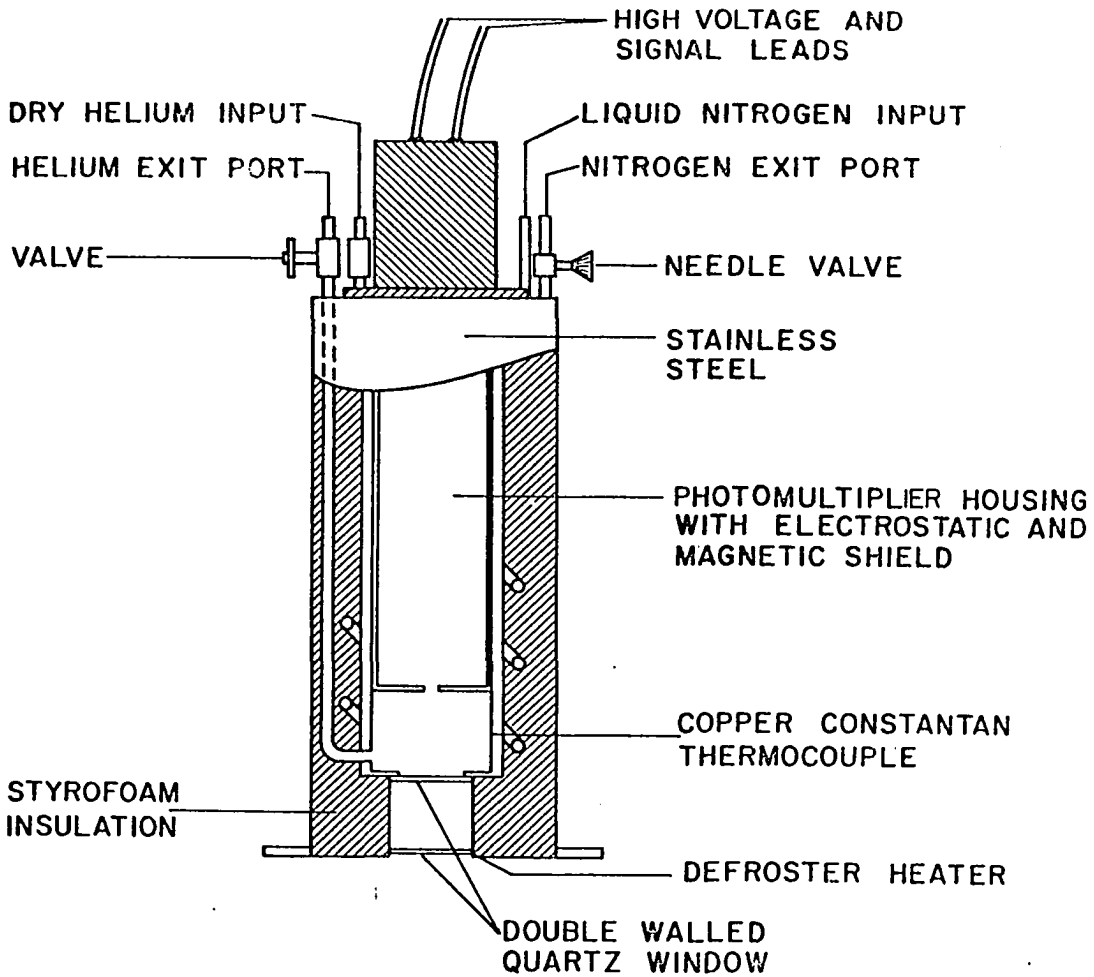

Figure 14. Andonian photomultiplier cryostat-housing

maintained free of water condensation by a 4 watt, electrical heater. A copper-constantan thermocouple (#36 gauge) which was located near the photomultiplier cathode permitted potentiometric temperature measurements (Rubicon Company, Philadelphia, potentiometer with a reference copper-constantan thermocouple in a 0°C, ice-water bath). The cooling cycle from ambient temperature to near liquid nitrogen temperature usually was about two hours long, and some regulation was possible through use of the needle valve on the nitrogen exit port.

An electrostatic and magnetic shield was available for use with the FW-118 photomultiplier. The circular aperture near the photocathode was 3/8 of an inch in diameter. The potential on the shield was the same negative, high voltage applied to the photomultiplier cathode.

The size and bulk of the cryostat required special mounting considerations. Optical coupling with and mounting onto the spectrometer were achieved in the manner depicted in Figure 15. A spherical achromatic lens (Flint-crown glass doublet, coated achromat of focal length 54 mm and diameter 29 mm, Edmund Scientific Company, Barrington, New Jersey) was employed to converge the exit-slit light beam and maintain a

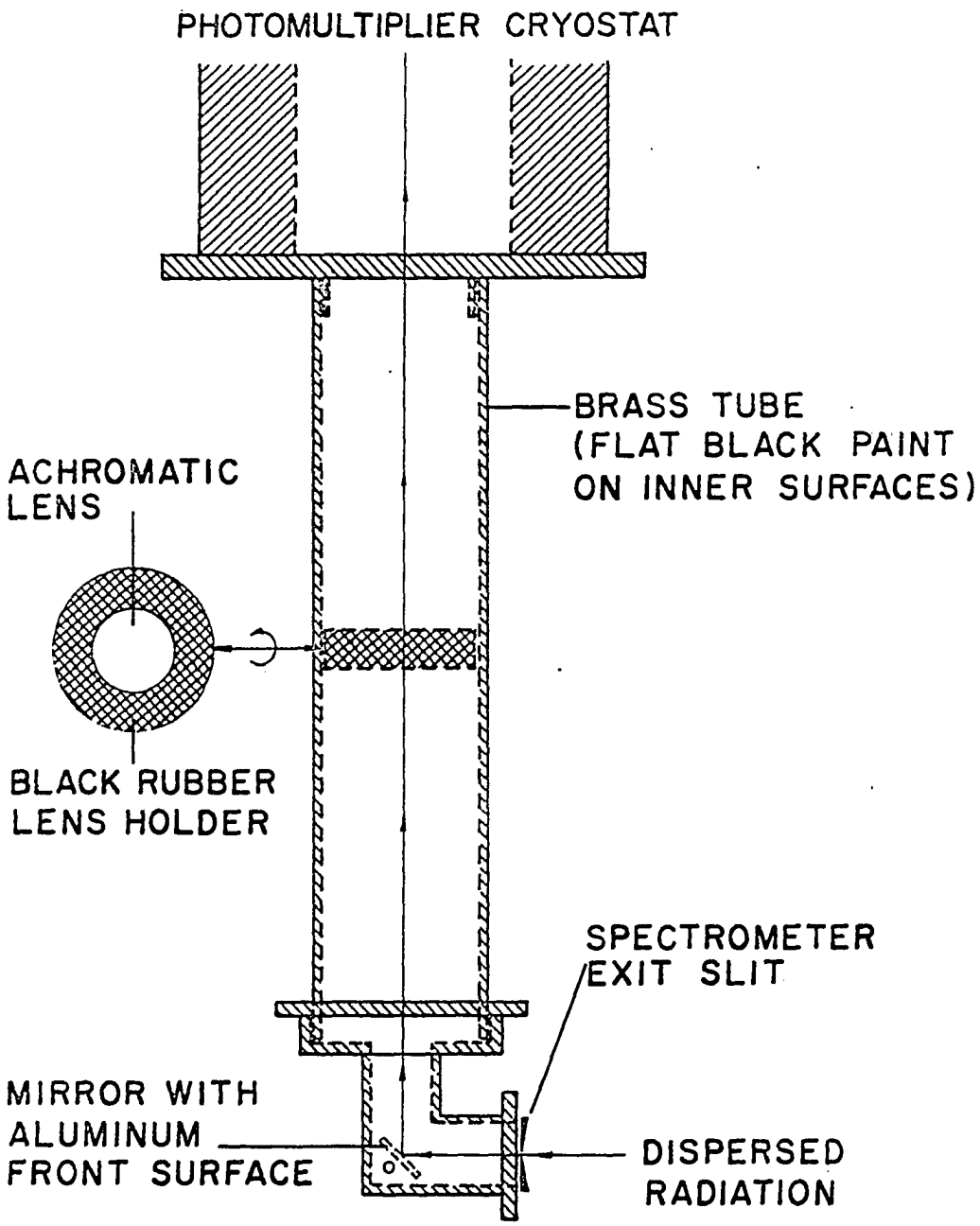

Figure 15. Optical system for coupling cryostat-housing with spectrometer

constant flux cross-section on the photocathode for the 6000 to 9000 Å spectral region. All inner surfaces of the transfer tubing were painted flat black to minimize reflection. Resistors in the respective voltage divider bridges were embedded in "potting" compounds to prevent water condensation across the electrical contacts.

3. Amplifier-recorder system

A Stabline automatic voltage regulator (model 1E5101R, Superior Electric Company) provided a stable, ac voltage supply for all electronic units in the system. The regulator was specified to maintain an output voltage of 115 volts rms $\pm$0.1 percent over an input range of 93-135 volts.

A regulated photomultiplier power supply (type S-325, NJE Corporation) provided an output of 500 to 2500 volts dc at 0 - 10 milliamperes, with a specified static load regulation of 60 millivolts and recovery time of less than 1 millisecond.

Spectral-line peak intensity measurements were accomplished with a Keithley model 410 micro-microammeter (Keithley Instruments). This vacuum tube electrometer was designed and constructed especially for measuring small currents and provided full scale ranges from 10^{-3} to 3×10^{-13} ampere. Accuracy was specified to be within 4 percent, and amplifier

noise was stipulated to be 30 millivolts rms at the output terminals regardless of the gain setting.

A Bristol model 590, wide-strip, two pen, Dynamaster recorder (The Bristol Company) was used for signal recording of spectral scans. Recorder time constant was determined to be about one second.

4. Direct-current integration system

One of the basic values of a direct-current integration method is that the length of measurement of a photocurrent can be increased to such an extent that appreciable improvements in signal-to-noise ratios can be gained. In other words, storage of a current on a capacitor produces an averaging or cancelling effect on random fluctuation components of the current. Thus, the ability to measure a small electrical signal, such as a photocurrent, should be increased by an integration method. In view of this information, an integration measuring system was chosen for this investigation. A block diagram sketch of the equipment arrangement for spectral scans and dc integrations which was utilized in this investigation is presented in Figure 16. The ac voltage regulator employed and depicted in this diagram was a 2 KVA, Sorenson

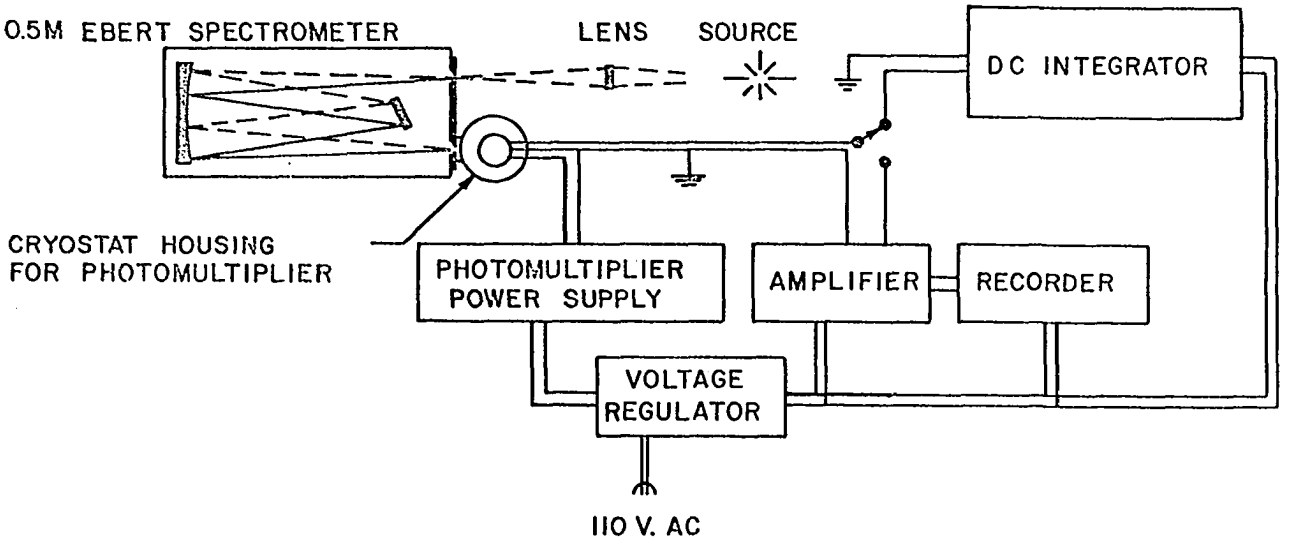

Figure 16. Direct-current spectral scanning and integration system

model 1750 (Sorenson and Company Incorporated, Stamford, Connecticut). Integration of photocurrents was performed with a Jarrell-Ash "Sequential Atomcounter Electronic System" (model 66-002, Jarrell-Ash Company, Newtonville, Massachusetts). Spectral lines were located with the aid of the panel-mounted microammeter which indicated the continuous output current from the photomultiplier. Entrance and exit slits of 25 μ width were used. Precise electrical timer-switches governed the 30 sec time interval during which a dc signal from a photomultiplier was fed into the integrating circuit. Signal integration was accomplished by storing charge on a low-leakage capacitor which is referred to as a channel capacitor. This charge was equal to the current-time product which is proportional to the total current produced by dark current and relative, optical background and line intensities. After charging, the capacitor was discharged through an analog-digital converter, where the resulting current was converted to voltage pulses and then counted on a four decade scaler. The displayed scaler count was the number of times the converter integrating capacitor was recharged to a specific level by the channel capacitor.

IV. RESULTS AND DISCUSSION

A. Image-Dissector Direct-Reading System

In order to set forth a general characterization of operational capabilities and explicit evidence attesting the ability of the image-dissector direct-reading method to provide quantitative information, a number of properties of the system which are important to the analytical spectroscopist were established.

1. Spectral resolution

The first of these properties of concern was the ability of the image-dissector spectrograph system to distinguish between individual neighboring spectral lines. This was determined by calculating the spectral bandpass of the 0.5 meter Ebert spectrograph and comparing this bandpass with measured spectral line widths of neon lines from a dc-operated hollow cathode source.

Single-sweep oscilloscope displays of several neon lines from the first order spectrum appear in Figure 17. Line widths at half-height are about 1 Å. This value compares well with the calculated spectral bandpass of 0.8 Å for a 50 μ exit slit. However, in this instance, the slit of 50 μ width was

Figure 17. Oscilloscope displays of selected, neon lines from a hollow cathode lamp

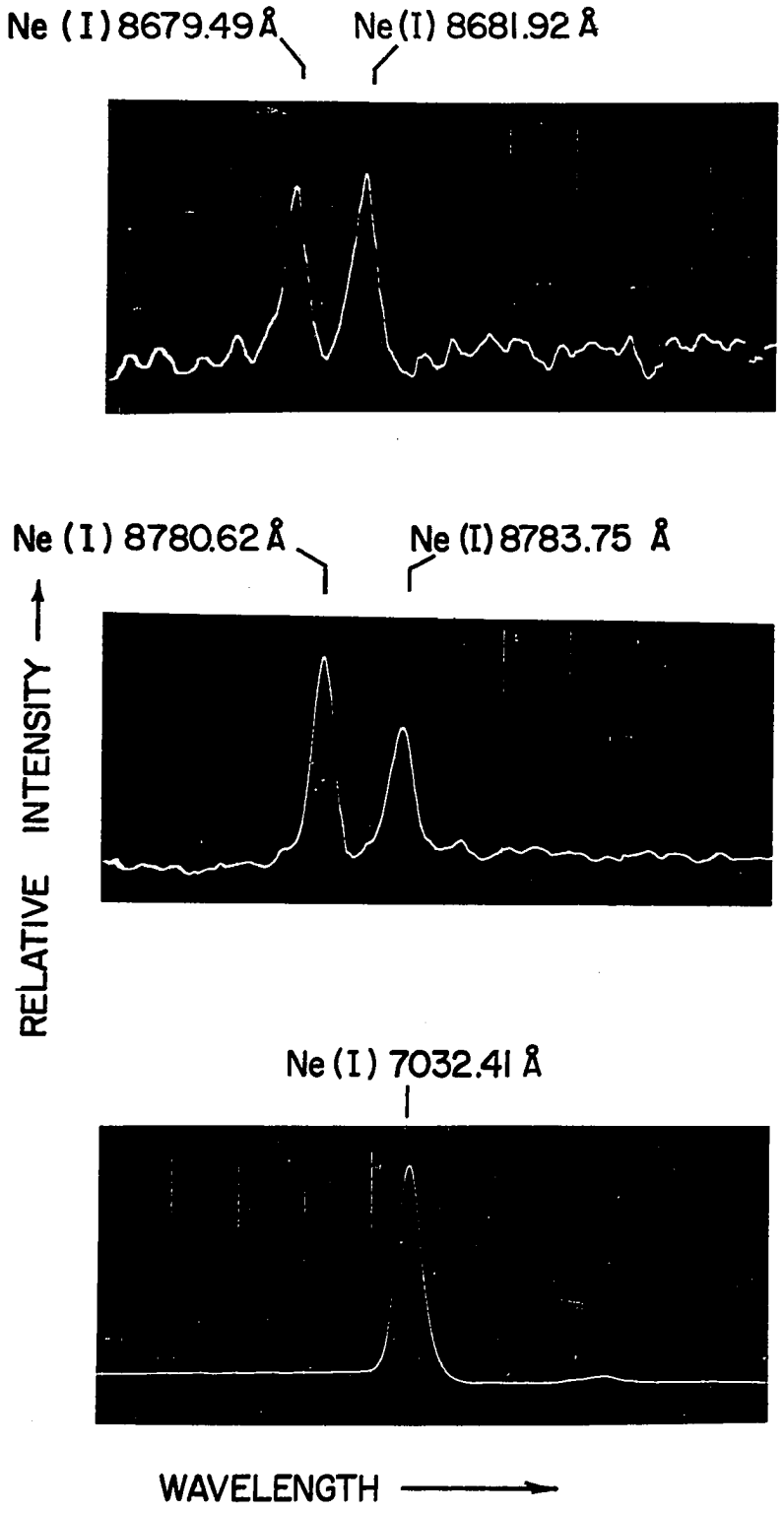
Ne (I) 8679.49 Å
Ne (I) 8681.92 Å
Ne (I) 8780.62 Å
Ne (I) 8783.75 Å
RELATIVE INTENSITY
Ne (I) 7032.41 Å
WAVELENGTH

the internal aperture of the image dissector. The well-resolved Ne(I) lines which are illustrated in the top photograph are 2.43 Å apart. These low-intensity, first-order, lines are separated by only 0.15 mm on the photocathode surface.

In addition to resolution, some indication of single-sweep signal-to-noise ratios appears in the photographs of oscilloscope traces of Figure 17. The relative intensities of the spectral lines shown in each of the three photographs increase from the pair illustrated in the top photograph to the neon 7032.41 Å line of the bottom oscilloscope display.

2. Separation of closely adjacent spectral lines with the gating function

The next characteristic of prime importance to be determined was the capability of this system to electronically separate spectral line pulses. This electronic function is analogous to the problem encountered in classical direct-reading spectroscopy of placing exit slits along the focal plane of a spectrograph in order to separate adjacent spectral lines. However, instead of the mechanical difficulties and limitations in positioning slits, mirrors and photomultipliers, the image-dissector direct-reading system is limited by the

gate pulse width and the electronic stability of the individual sweep and trigger circuits.

Although no actual situation in which analytical data were required for one of two spectral lines that were within 2 to 3 Å of each other was encountered in the present analytical investigations, such gated separations were possible, and an example is illustrated in Figure 18. The photograph A shows the total, single-sweep oscilloscope display of two neon lines from a dc-operated hollow cathode lamp. Gate width and position were then changed in order to isolate the line-pair (B) or either of the two lines of the pair (C and D).

3. Single-sweep, gated line integrations

Use of the Tektronix gating adapter with the type "O" plug-in operational amplifiers also enabled gated, single-sweep integrations of the pulse areas that correspond to spectral lines such as the one illustrated in the oscilloscope traces of Figure 19. The left hand base of the neon line (A) was electronically clamped at a set level for the line and background integrations (B and C, respectively). At the end of the single oscilloscope sweep, the plates of the feedback capacitor were automatically shorted and the integrating

Figure 18. Oscilloscope displays which illustrate gate positioning for selective, line integrations

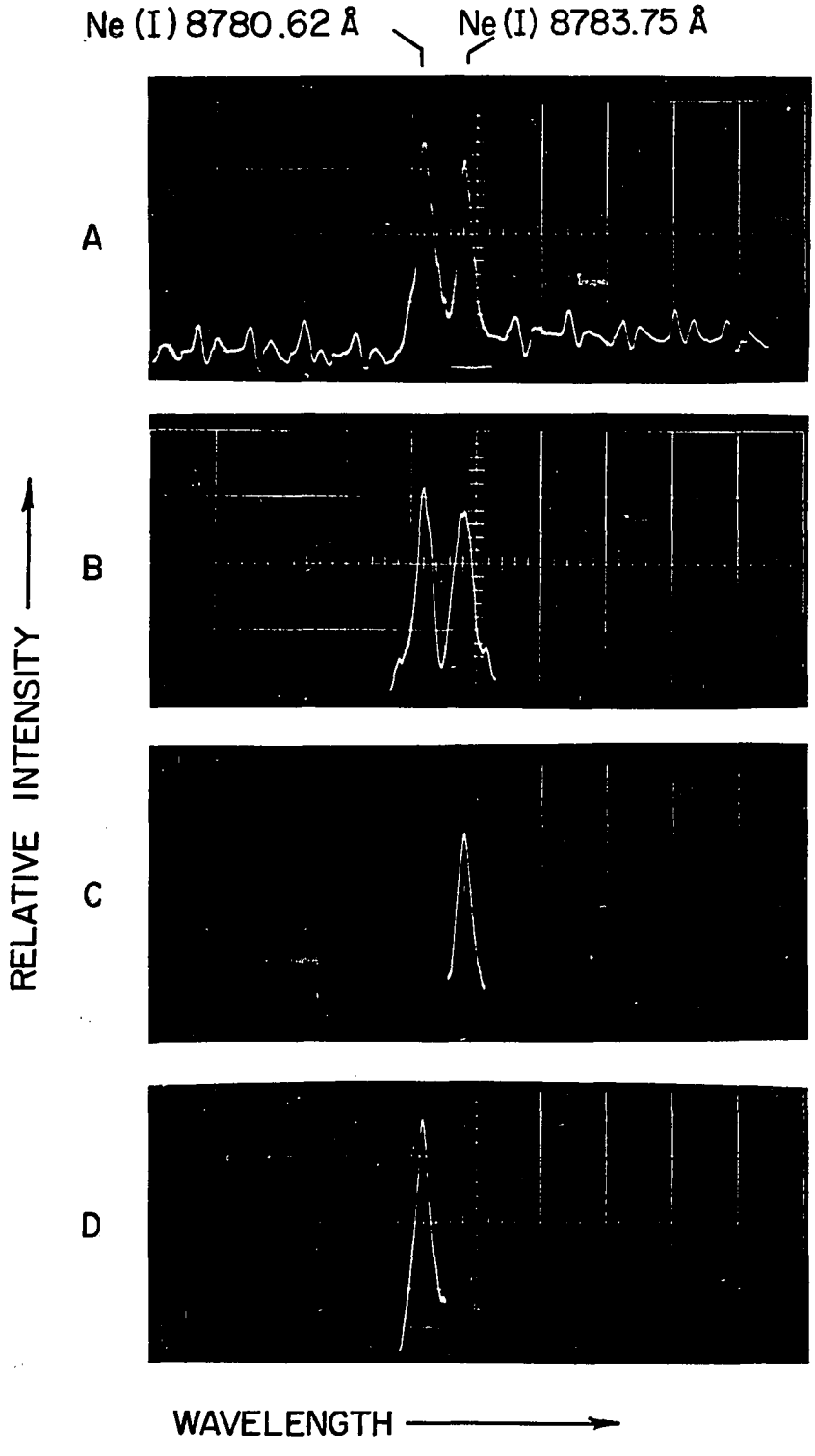
Ne (I) 8780.62 Å
Ne (I) 8783.75 Å
A
B
C
D
RELATIVE INTENSITY
WAVELENGTH

Figure 19. Oscilloscope displays of a gated, single-sweep integration

A. Ne (I) 8377.61 Å Line

2.5 mV/cm

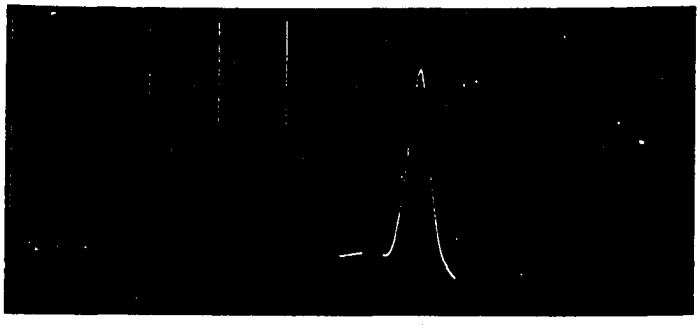

B. Gated, Single-Sweep Integral

10 mV/cm
0.01 μf

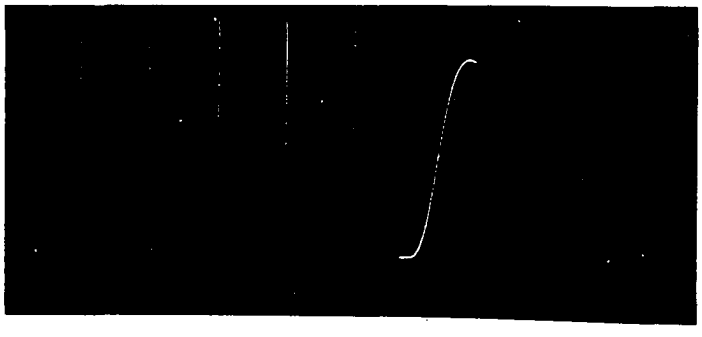

C. Gated, Single-Sweep, Background Integral

10 mV/cm
0.01 μf

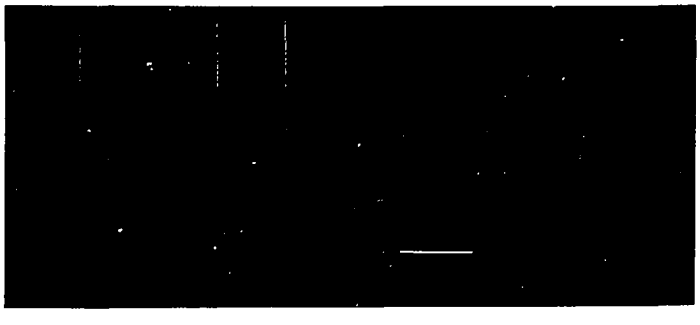

WAVELENGTH ⟶

circuit (Figure 12) was ready to perform another independent integration.

Figure 19 also demonstrates that a true area integration of the spectral line pulse was performed by the operational amplifier, for the change in the value of the integral with wavelength corresponds to the change in pulse area with wavelength. This type of integral stored for many sweeps over a spectral line constitutes the area-time integral that was referred to in previous discussions.

4. Oscilloscope displays of alkali metal spectral lines from a premixed oxy-acetylene flame

Before preparing analytical calibration curves from spectral lines of the common alkali metals, evidence of line identities, relative intensities and signal-to-noise ratios in the spectra from a premixed oxy-acetylene flame was obtained. Photographs of single-sweep oscilloscope displays which present this evidence appear in Figures 20 and 21. Maximal advantage of the S-1 response photocathode was attained through use of the intense resonance lines of the alkali metals which occur in the red region of the spectrum. The solution concentrations employed to produce the observed relative line intensities are indicated with each spectrum in

Figure 20. Oscilloscope displays of Li, Na and K lines from a premixed, oxy-acetylene flame

A. Li (I) 6707.84 Å 1 μg/ml

2 mV/cm

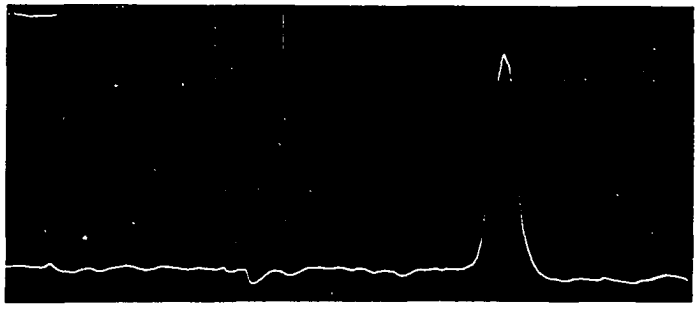

B. Na (I) 5889.95, 5895.92 Å 5 μg/ml

0.9 mV/cm

C. K(I) 7664.91 Å 12 μg/ml

0.75 mV/cm

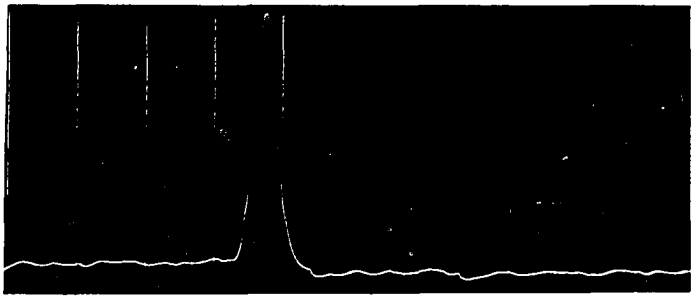

WAVELENGTH ⟶

Figure 21. Oscilloscope displays of Rb and Cs lines from a premixed, oxy-acetylene flame

A. Rb (I) 7800.23 Å 10 μg/ml

0.4 mV/cm

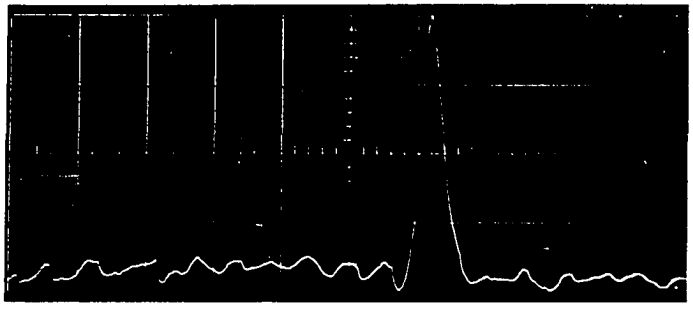

B. Cs (I) 8521.10 Å 100 μg/ml

1 mV/cm

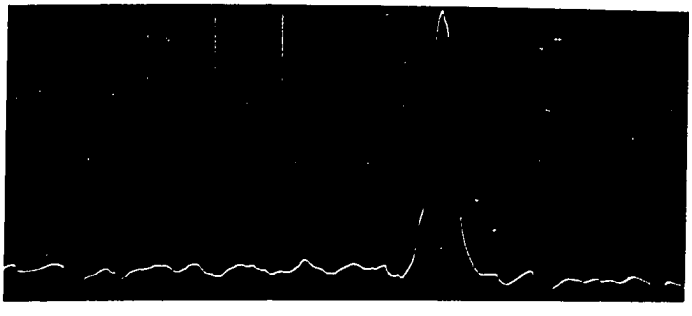

WAVELENGTH ⟶

Figures 20 and 21. The voltage scale indicated with each photograph refers to the drop across the preamplifier input.

5. Analytical calibration curves

The ability of the image-dissector direct-reading system to provide quantitative information is illustrated by the analytical calibration curves shown in Figures 22 and 23. Units for the pulse area-time integrals of spectral lines from the premixed oxy-acetylene flame were made arbitrary but self-consistent for each spectral line and element. Since the magnitude of the voltage stored on the integrating capacitor was directly proportional to the number of sweeps, it was convenient to put all these recorded voltages onto a common basis for a chosen number of sweeps. Linearity and unit-slope of the curves are apparent. The sodium doublet lines were suitably separated in time (Figure 20, B) so that gated integrations of either line or both lines were possible. For these data, the scanning rate of the image dissector was 10 sweeps per second, and integrations were performed for intervals which corresponded to 25 to 300 sweeps.

Although not affirmed by the curves presented in Figures 22 and 23, Chaney (100) observed photographically that analytical curves based on area-time integrals of spectral

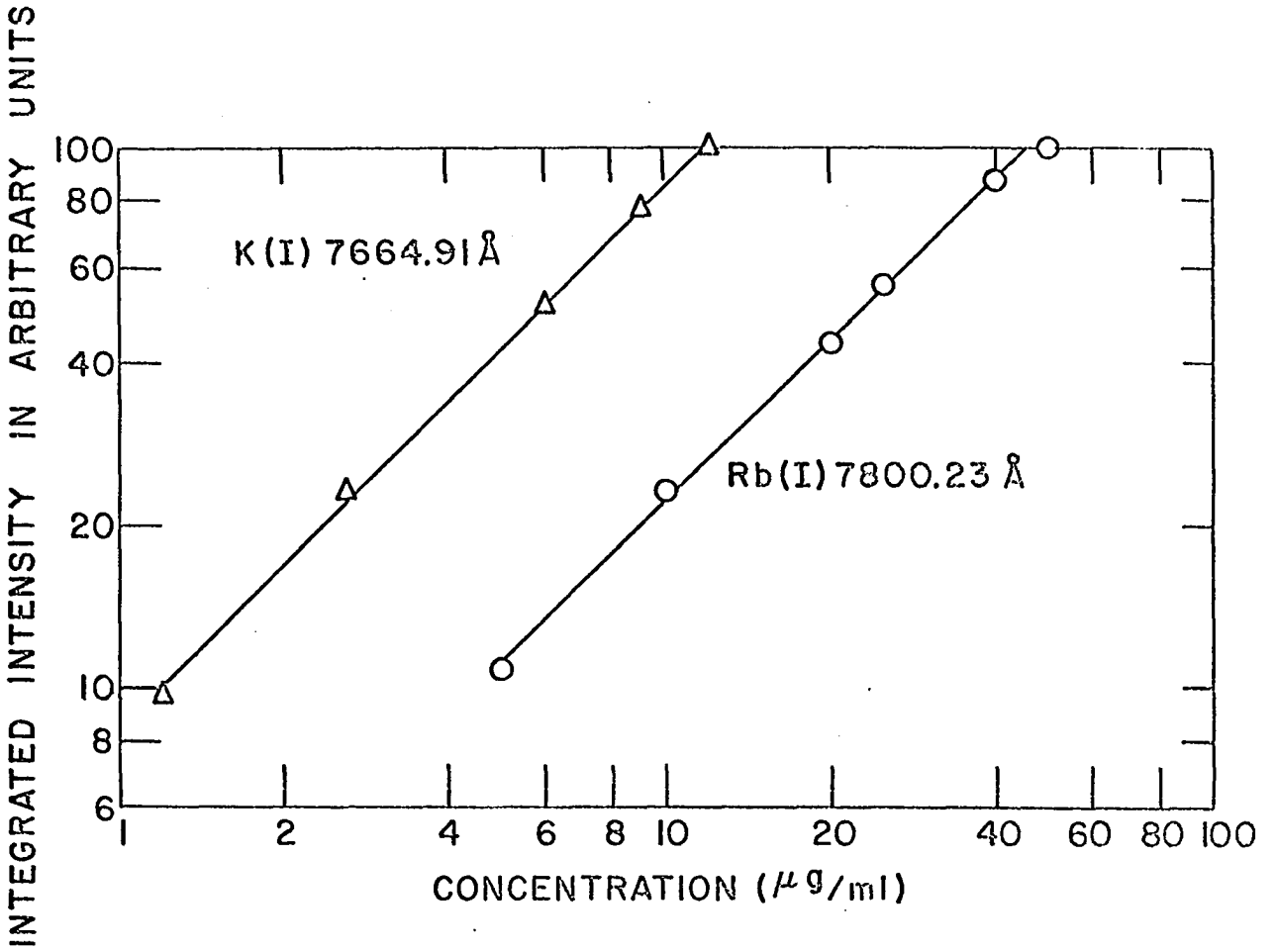

Figure 22. Potassium and rubidium analytical calibration curves

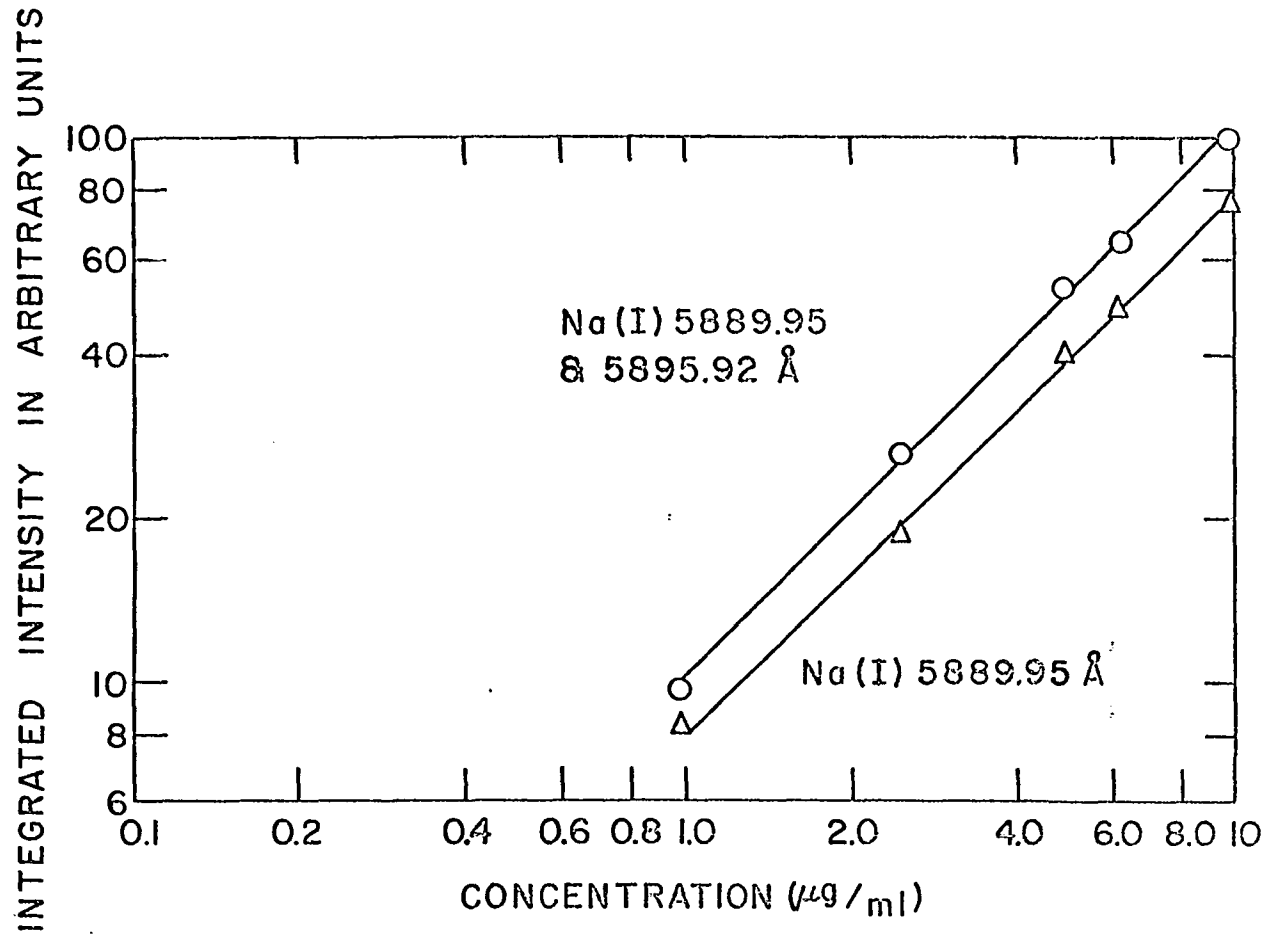

Figure 23. Sodium analytical calibration curves

lines were unaffected by self absorption and exhibited linearity over a greater concentration range than analytical curves derived from line peak-height measurements. A similar linearity over wide concentration ranges should be expected with the image-dissector direct-reading system. In addition, small changes in optical focus or the position of a line image on the photocathode of an image dissector should produce no change in the pulse area-time integral of a spectral line.

6. Precision of measurements

The capability of a system to reproduce an individual measurement is equally as important as the ability to make the measurement itself. The reproducibility of integrated intensities in the analytical curve for rubidium emission from the primary reaction zone of a premixed oxy-acetylene flame is indicated in Figure 24. Each point, which represents the mean value from ten integrations, and the average deviation are indicated in this plot. Precision is better for higher rubidium concentrations and generally appears comparable to that obtained in a similar analytical calibration curve produced with the image dissector operating as a conventional dc detector (Figure 25). For example, the standard deviations in the values for spectral line height and pulse area-time

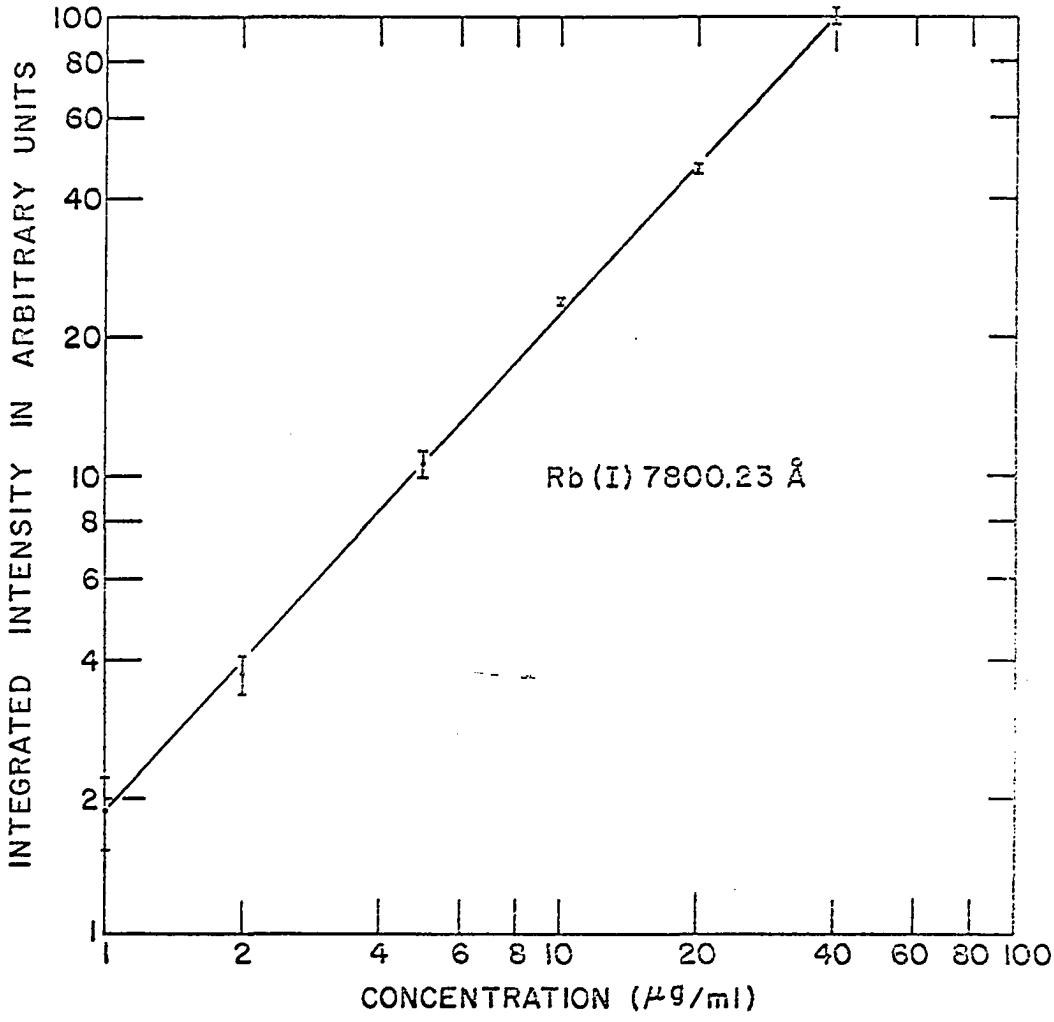

Figure 24. Rubidium analytical calibration curve with image-dissector direct-reading system

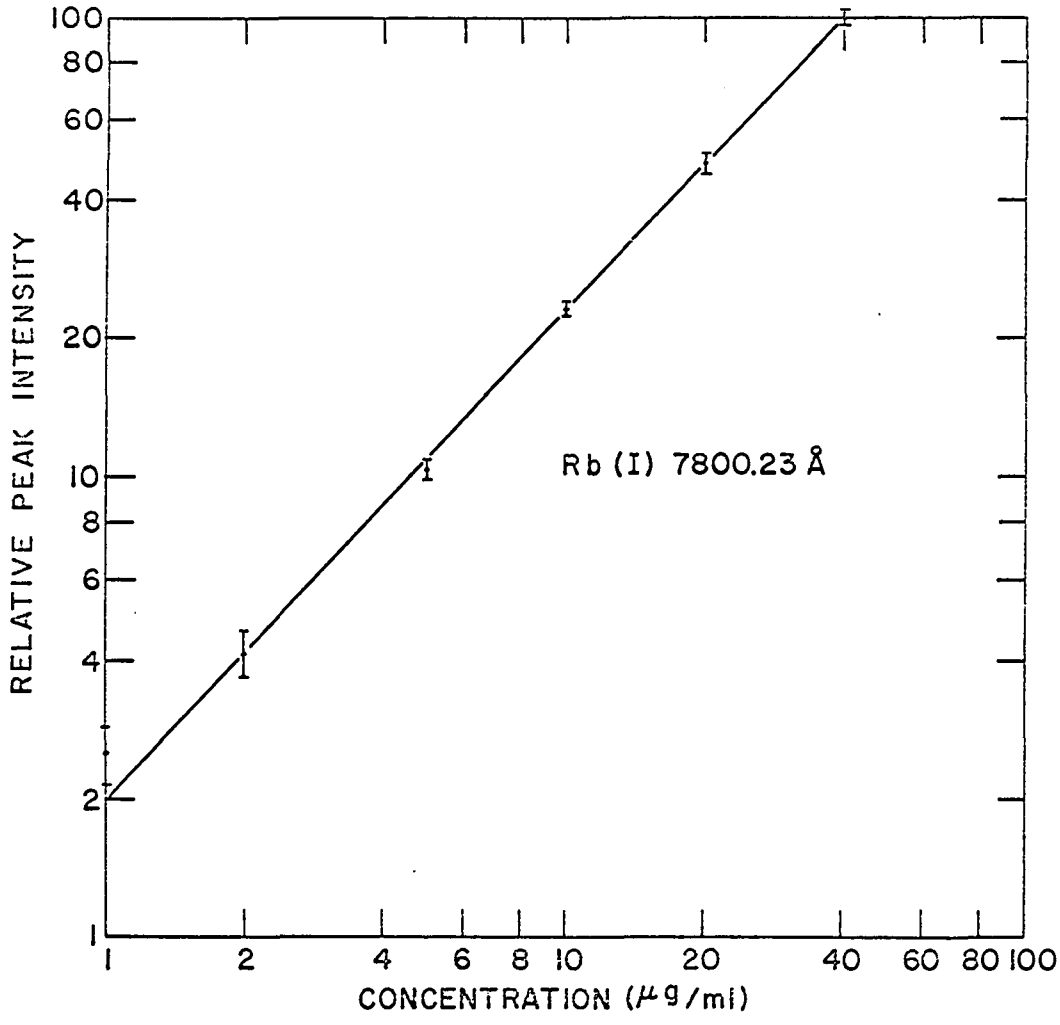

Figure 25. Rubidium analytical calibration curve with spectral-scanning system

integrals at the 2 μg/ml rubidium concentration are ±7.1 percent and ±5.4 percent, respectively. Normally, precision for the measurements of integrated signals should be expected to be significantly better than the reproducibility observed with the conventional scanning technique because the effective time for each measurement is longer by the former method. This expectation should be particularly noticeable in situations where the signal-to-noise ratio is low, such as the situation for the 2 μg/ml rubidium concentration. However, the intrinsic inability of the Philbrick operational amplifier to reproduce voltage integrals to better than ±1 percent and the uncontrolled current leakage off the integrating capacitor through the recorder input were two important factors which contributed to an unsuitable illustration of this effect. Use of a wide-range, electrometer-input digital voltmeter in place of the recorder readout should reduce leakage from the integrating capacitor, provide a more convenient readout and facilitate the attainment of calibration points for analytical calibration curves for which a consistent noise averaging for every signal integration has been provided.

In order to obtain signal integrals over time periods that will allow the establishment of reliable analytical

calibration curves and ensuing analyses, suitable stability of the detector and accompanying electronics is required. Drift or instability is usually the result of photomultiplier fatigue effects or changes in vacuum tube characteristics with temperature variations and aging. The importance of changes in the zero offset voltages in operational amplifiers on drift of an integrated signal value was discussed in a previous section.

The maximum variation of a "300-sweep" integral of the Ne(I) 7032.41 Å line from a hollow cathode lamp over a five hour period was determined to be two percent from an initial value obtained after a one hour stabilization period. The standard deviation from the mean integral value during this interval was about ± 0.9 percent. No drift of output signal from the image-dissector photomultiplier that could be attributed to fatigue effects was observed.

Drift properties of the present image-dissector direct-reading system could be improved with two changes. Firstly, the battery supply for the preamplifier should be replaced with a stable electronic power supply, such as the Tektronix model 125. Gain of the preamplifier was very dependent on the current supplied to filaments of the vacuum tube

amplifiers and drifted with changes in the capability of the battery to supply a constant current. Secondly, further stability of the integrating system should be obtained upon exclusive use of high-frequency, chopper-stabilized operational amplifiers. Variations in zero offset voltages for this type of operational amplifier are much lower than the drifts incurred with non-stabilized amplifiers such as those in the Tektronix plug-in module.

7. Other possible applications of the image-dissector photomultiplier

Although the primary concern of this section was to elucidate the characteristics of the image-dissector photomultiplier as a detector in direct-reading spectroscopy, other applications are readily apparent. The property of the image-dissector photomultiplier system to make repeated and reproducible, non-mechanical spectral scans suggests a convenient application to signal averaging techniques in optical spectroscopy. Signal averaging refers to an electronic method for improving the signal-to-noise ratio for the output of any system that generates an electrical signal from a repeated sweep action. A channel analyzer is utilized to effectively divide each sweep spectrum into distinct time gates which

correspond to each of the channels. Upon storage of signal in this sytem over many sweeps, the effective algebraic addition of random noise components reduces the background fluctuation level, while the always-positive pulses which correspond to spectral lines grow in magnitude. Thus, a large sacrifice in time can produce very significant increases in signal-to-noise ratios.

Another application as detectors in direct-reading, atomic absorption spectroscopy system is possible. Either hollow cathode or spectral continuum lamps could be used as primary sources. Also, simultaneous atomic absorption and emission measurements are feasible with a rapid-scanning image dissector and a modulated, primary light source. In this instance, the scanning and chopping frequencies must be quite different so that the respective output signals from the detector can be separated and a sufficient number of pulse integrations performed during each portion of the chopping cycle.

Used with a driven sweep and variable time-delay, the image dissector could be employed in time-resolved spectroscopy. In this case, the optical emission source unit would provide the pulse to trigger the deflection coil sweep.

Many other feasible applications, such as a spectral alignment monitor for conventional direct-reading systems, and uses in the fields of temperature measurements and kinetics also exist.

B. Performance Data on the FW-118 and C70007A Photomultipliers

Since one of the primary difficulties encountered in direct-reading spectroscopy with S-1 response photomultipliers centers on the high dark current, a reduction of this dark current through the cooling of these photocathodes appears to be a simple, logical step toward a more ideal system. However, this step does not alleviate the classical problems with exit slits and spectrum shifts which result from temperature, pressure and humidity changes. In fact, air temperature gradients produced by the presence of coolants around the focal plane of a direct-reading spectrograph generally should be expected to compound slit positioning problems. Nevertheless, some preliminary investigations of low-temperature characteristics of the FW-118 and C70007A were conducted in an effort to provide comparative information between these

photomultipliers, and the direct-current and pulse integration methods.

1. Dark current dependence on cathode temperature

The precipitous drop in dark current with decreasing temperature for both S-1 response photomultipliers is illustrated in Figure 26. Dark currents of these photomultipliers were diminished by about five orders of magnitude over an approximate 180°K change. Since the data points were obtained by continuously recording dark current on a strip-chart recorder during the cooling cycle, true thermal equilibrium most likely did not exist for the upper portions of the curves. However, as the cooling rate decreased and a minimal cryostat temperature slowly was attained, the recorded dark currents approached equilibrium values. For the applied voltages indicated in Figure 26, current amplification of the FW-118 was about one hundred times that of the C70007A.

2. Spectral scans of oxy-acetylene flames in the 6000 to 9000 Å spectral region

A very apparent application of refrigerated, S-1 response photomultipliers was to the conventional spectral-scanning technique in which a strip-chart trace of total photocurrent was produced by rotating the spectrometer grating in order to

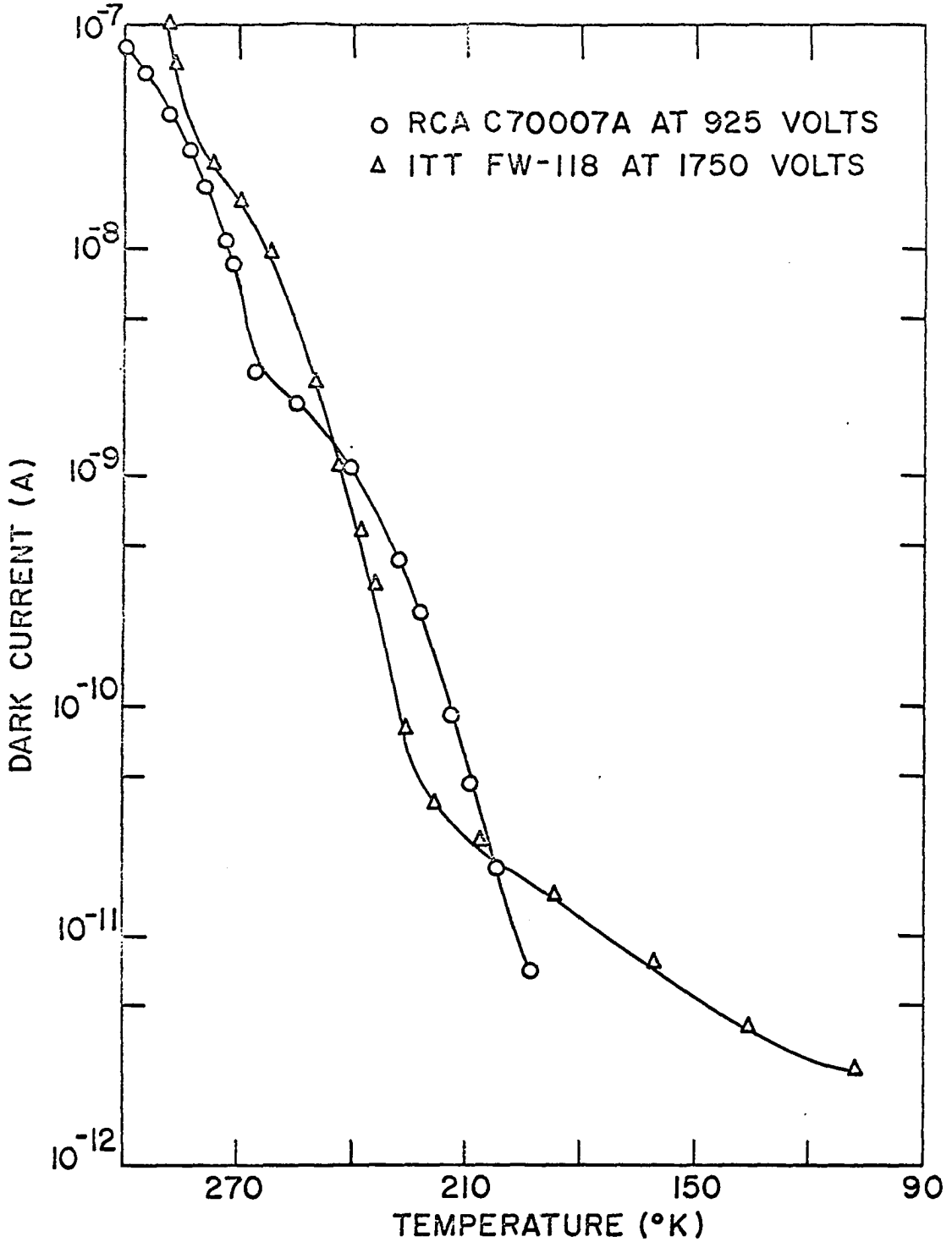

Figure 26. Dark current-temperature curves for two S-1 response photomultipliers

move the spectrum across a single exit slit. In this situation, the detector permitted sensitive photoelectric observations of radiation in the red region of the spectrum which were not superposed on a high dark current signal.

Spectra from various zones of premixed, oxy-acetylene flames which exhibit the general background radiation levels and band structure are shown in Figure 27. These traces were obtained with a FW-118 which was operated at 125°K. At this temperature, dark current from the photomultiplier was negligible relative to the photoelectric signals that originated from flame radiation. Even the lowest photocurrents produced by the refrigerated FW-118 were about 200 times greater than the dark current level. The reference to a less fuel-rich flame stoichiometry in the upper spectrum of Figure 27 indicates that the interconal zone was collapsed to a layer which was indistinguishable from the primary reaction zone. For this particular spectrum, the observed radiation was sampled from the region immediately above the primary reaction zone.

These data, however, do not convey any direct, quantitative information on which a comparison between photomultipliers or integration systems may be based. An inroad to such

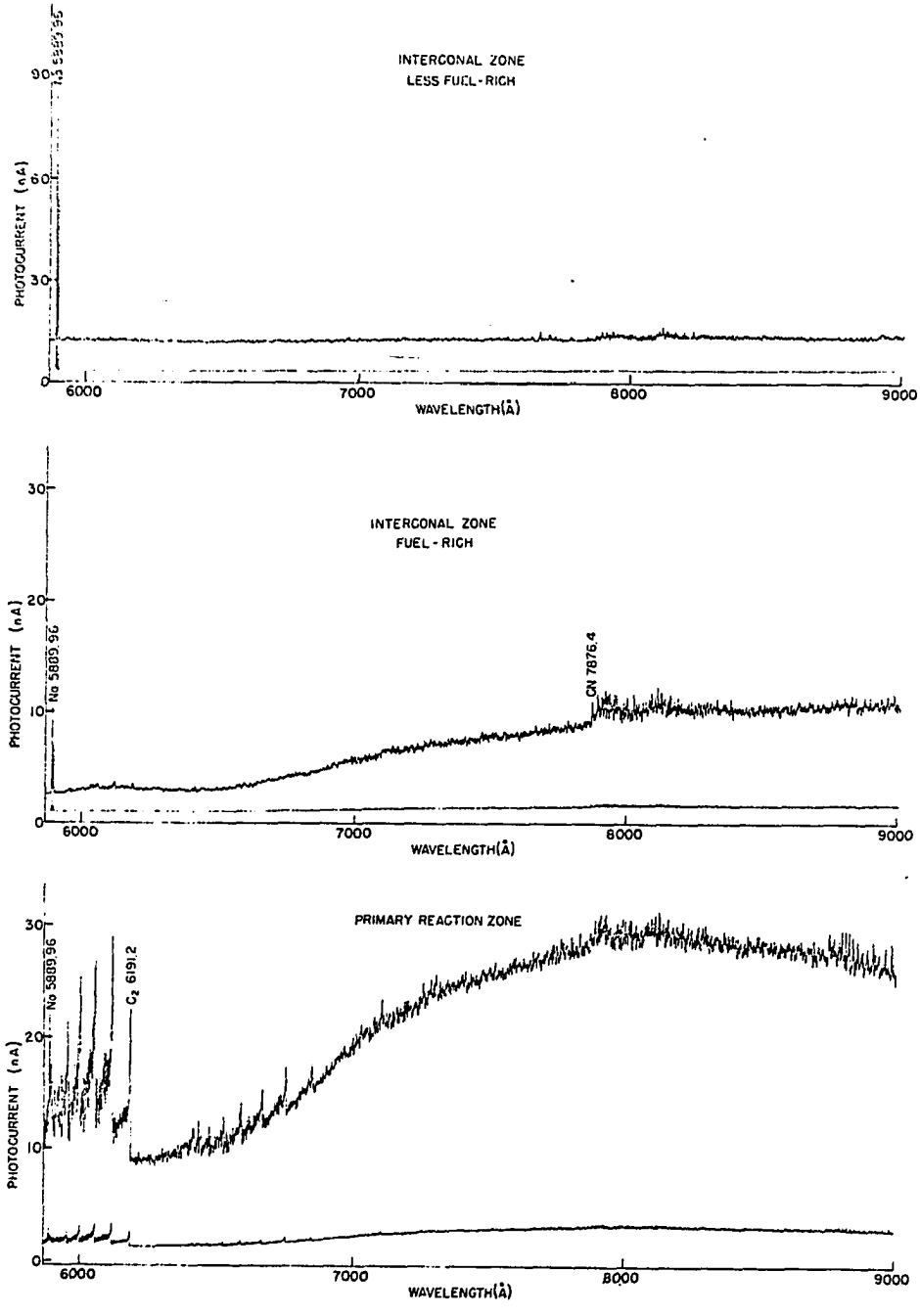

Figure 27. Spectra from zones of premixed, oxy-acetylene flames obtained with a cooled FW-118 photomultiplier

contrasts was sought in the detection limit and associated concepts which form the subject of the following section.

C. Detection Limits

Prior reference to the signal-to-noise ratio as a figure of merit for an electronic detection system was made in Section II-B. Since the detection limit is defined to be a concentration of an element in solution required to produce a stipulated, threshold, signal-to-noise ratio, it too can be construed to be a measure of merit for a total optical-electronic-source system.

Strip-chart recordings of wavelength versus relative, spectral-line intensity, which are obtained by scanning a spectrum across the exit slit of a spectrometer and recording the electronically amplified, dc signal from a photomultiplier, afford a ready definition of the detection limit. A standard definition, which has been adopted by a number of investigators in both flame emission and flame, atomic absorption spectrometry (99, 101-105), assigns the detection limit to be that concentration of element in solution which upon nebulization into a flame will produce a line signal (absorption or emission) that has an average magnitude

equivalent to a constant times the standard deviation in the immediately adjacent, background signal. The fluctuation in the background trace is attributable to flame fluctuation, band structure from combustion species and noise derived from the electronic detection and amplification system. Spectral line intensity and background fluctuations are both visible and very real quantities, and this aspect makes such a definition quite practical and meaningful. The value chosen for the constant is usually 2 or 3 and reflects the desired statistical confidence level.

In situations where the dc signal from a photomultiplier is integrated for relatively long time intervals, the definition becomes more complicated because of the character of the numbers which are obtained and the existance of electronic drift, which is not particularly apparent in scale-expanded, strip-chart recordings. Logically, one should expect better detection limits to be obtained by an integration method, because capacitor storage of a background current that has truly random fluctuation tends to "average" this noise to zero level and accordingly improve the observed signal-to-noise ratio. Ideally, then, one should be able to detect almost any quantity of an excitable element in solution

if the integration process were sustained for a sufficiently long period and if a finite probability of exceeding the amplifier threshold by the line signal in this interval were extant. However, this is not the case for a dc-coupled system or any detector-amplifier system which shows drift in output signal with time. Firstly, there will always be a positive background signal (photomultiplier dark current plus background emission signal from the source) which can build to an appreciable integral value during an integration period. Since the storage and counting capacities of any electronic integrator are limited, the integration intervals for background and signal plus background accordingly are limited. Secondly, the integration process must be performed during a period over which no appreciable drift occurs. Otherwise, a spurious integral component due to system drift will be considered a portion of background or signal integrals. Both of these effects are very pronounced for S-1 response photomultipliers, for the red-sensitive photomultipliers typically exhibit very high dark currents and a significant drift due to fatigue effects.

A conditional definition of detection limit is possible for integration counts (from a scaler digital readout) of

background and line signal. If a sufficient number of samples of integrated background intensities and integrated line intensities can be obtained in an interval of such a span that drift is negligible, a legitimate measure of a detection limit based on the average signal and statistical background fluctuation magnitudes can be made. However, there is an additional stipulation necessary to make the detection limit extrapolation a valid one: a significant fraction of the integrated background signal must originate from the signal source. If this last requirement is not met, the background count statistics refer only to the ability of the integration system to reproduce integrated, photomultiplier dark current measurements. If it were possible to reduce this dark current to sufficiently low levels so that the photomultiplier gain could be increased to provide a higher background signal level from the optical source, more meaningful detection limits could be obtained.

This latter observation suggests the use of photomultipliers with limited cathode areas, such as the FW-118, or the refrigeration of a photomultiplier to reduce dark current output. Both of these approaches were attempted with S-1 response photomultipliers. Ambient temperature detection

limits obtained with the FW-118 and C70007A for dc integrations are presented in Table 6. Efforts to determine detection limits with the same detectors at low temperatures were not successful because of severe and uncontrollable drift that most likely resulted from lack of good temperature control and fatigue effects. Additionally, the FW-118 began to produce spurious pulses that were later found to be attributable to the formation of a cesium glow-discharge within the photomultiplier glass envelope and near the base pin contacts. All data obtained with the FW-118 and reported in Table 6 were procurred during the first 100 hours of tube operation and before the discharge effect on noise levels at high, applied voltages was observed.

The very high dark current of the C70007A overshadowed background signal from the flame, and thus, fluctuation measurements primarily reflect reproducibility of dark current integrations. Also, the signal-to-noise ratio properties of this tube were not optimal, for the focusing electrode had to be disconnected after repeated sparking to the cathode occurred. Differences in the detection limits obtained with the FW-118 and C70007A are roughly indicative of the lower

Table 6. Detection limits from spectra of premixed, oxy-acetylene flames

Element	Wavelength[a] (Å)	Detection limit (μg/ml) by dc integration		spectral scanning	
		FW-118	C70007A[b]	FW-118	Literature (102)[c]
Li	6707.84	0.002	0.03	-	0.000005
Na	5889.95	0.02	0.2	-	0.0002
K	7664.91	0.03	1	-	0.005
Rb	7800.23	0.01	3	-	0.003
Cs	8521.10	0.3	10	2	0.01

[a] M.I.T. Wavelength Tables (106).

[b] Operated without focusing electrode connected.

[c] Recalculated for an average signal level equal to three times the standard deviation in background.

dark current and noise properties of the former photomultiplier. Although the C70007A photomultiplier was not operated in an ideal fashion, the detection limit results still approximately indicate the signal-to-noise ratio properties of the detector. The spectral-scanning detection limits recorded in Table 6 were determined with S-20 response (Li, Na, K) and S-1 response (Rb, Cs) photomultipliers of which the latter was a FW-118 operated at 125°K (102).

Unfortunately, these detection limit data were not sufficiently extensive at the time of writing to answer other questions of interest to the analytical spectroscopist. For example, the query into how much different the spectral-scanning detection limit values would be at ambient temperature upon utilizing this image dissector or special versions of the FW-118 with an internal slit-shaped aperture has not been answered.

Although the measurement time for the dc integrations (30 sec) indicates that an improvement in signal-to-noise ratio by a factor of about 3.5 ($\sqrt{30/2.5}$) over that of the spectral-scanning value (2.5 sec) (45, p. 257) should be obtained, such a trend, obviously, is not followed. The reasons for this seem to center on the higher quantum

efficiency of an S-20 response surface below 7800 Å and the ability to scale-expand by very large factors at a low band-pass (typically, about 0.5 Hz) with a dc, spectral-scanning method. Scale-expansion refers to the condition under which a suppression or bucking potential is applied ahead of the strip-chart recorder amplifier while the preamplifier is operated at very high gain in order to keep the recorder pen on scale. In this circumstance, the actual zero effectively is shifted off scale so that the recorder pen can operate in normal fashion on the strip-chart paper. Also, under this set of conditions, drift is not noticeable.

In the case of the integrations of voltage pulses from the image dissector, no signal analogous to dark current existed. Zero offset voltages of the gated and integrating operational amplifiers were commonly set so that no integral was obtained during the integration period of concern. This procedure allowed the production of unity-slope, analytical calibration curves (Figures 22 and 23) with no background correction. Thus, integrated background signals were not possible under practical operating conditions. Since there was no conceivable way to refer directly to background noise, a detection limit could not be based on the previously

described criteria which included a consideration of background fluctuation. If one attempts to use drift as the determining factor, that is, whether or not a certain concentration of element in solution will produce a voltage integral that is definitely not attributable to drift, the question of how long the integration interval should be reduces a detection limit derived from this basis to an arbitrary number. Therefore, no direct comparison of this pulse integrating system with the dc integrating system was possible.

V. SUMMARY

An S-1 response-type, image-dissector, multiplier phototube has been investigated as a detector in analytical emission spectroscopy. The role of this detector in a new approach to direct-reading spectroscopy was stressed. Associated current supplies for focus and deflection coils were built. The detector was attached to a 0.5 meter, Ebert spectrograph with a specially-constructed housing. Appropriate circuitry was assembled to allow an oscilloscopic display of a small spectral region and gated integrations of spectral line pulses by means of operational amplifiers.

Spectral resolution of 1 Å was attained in first order with an internal slit-shaped aperture of 50 μ width. Analytical calibration curves for some alkali metal emission lines from a premixed, oxy-acetylene flame were obtained. Precision of measurements and drift were studied. The image dissector permitted a non-mechanical, rapid-scan approach to direct-reading spectroscopy that eliminated some of the serious problems encountered with conventional, dc integration instrumentation. A discussion of the unique properties and other potential applications of this detector was presented.

Selected performance characteristics of two S-1 response-type photomultipliers in spectral-scanning and dc integration systems were compared for ambient and low temperature operating conditions. Alkali metal detection limits, which were based on integrated photomultiplier currents for ambient temperature operation of these detectors, were determined.

VI. LITERATURE CITED

1. Sawyer, R. A. Experimental Spectroscopy. New York, Prentice-Hall, Inc. 1951.

2. Brehm, R. K. and Fassel, V. A., Spectrochim. Acta, 6, 341 (1954).

3. Bullock, B. W. and Silverman, S., J. Opt. Soc. Am., 39, 200 (1949).

4. Benn, R. E., Foote, W. S. and Chase, C. T., J. Opt. Soc. Am., 39, 529 (1949).

5. Agnew, J. T., Franklin, R. G., Benn, R. E. and Bazarian, A., J. Opt. Soc. Am., 39, 409 (1949).

6. Andreev, V. L., Byul. Nauchn.-Tekhn. Inform., Tsentr. Nauchn.-Issled. Inst. Olovyan. Prom., 2, 54 (1962). Original not available, cited in Chemical Abstracts 61, 3a (1967).

7. Lundegårdh, H. G. Die quantitative Spektralanalyse der Elemente. Zweiter Teil. Jena, Verlag von Gustav Fischer. 1934.

8. Schunknecht, W., Angew. Chem., 50, 299 (1937).

9. Thanheiser, G. and Heyes, J., Spectrochim. Acta, 1, 270 (1939).

10. Jansen, W. H., Heyes, J. and Richter, C., Z. Physik Chem., 174, 291 (1935).

11. Dieke, G. H. and Crosswhite, H. M., J. Opt. Soc. Am., 35, 471 (1945).

12. Hasler, M. F., Iron Age, 159, 71 (1947).

13. Hasler, M. F. and Dietert, H. W., J. Opt. Soc. Am., 34, 751 (1944).

14. Coheur, P. and Hans, A., Congr. Group. Avan. Methodes Anal. Spectrog. Prod. Met., 11, 45 (1949).

15. Hasler, M. F., Davidson, E., Orr, H. and Barry, W. H., Mikrochim. Acta, 213, 596 (1955).

16. Crosswhite, H. M., Spectrochim. Acta, 4, 122 (1950).

17. Hasler, M. F. The Direct-Reading Analysis of Low Alloy, Tool, and Stainless Steels with the Quantometer. Unpublished Xeroxed paper presented at Conference on Instruments and Measurements, Stockholm, Sweden, Sept., 1949. Glendale, California, Applied Research Laboratories. 1949.

18. Barry, W. H. and Carrol, J. M., Proc. Colloq. Spectroscopicum Intern., 7th, 281 (1959).

19. Benussi, L. and Caroli, A., Rept. Colloq. Intern. (Venezia), 2nd, 97 (1951).

20. Breckpot, R. and Hainski, Z., Mikrochim. Acta, 213, 646 (1955).

21. Breckpot, R., Morris, J. and de Clippeleir, K., Rev. Universelle Mines, 15, 266 (1959).

22. Dickens, P. and Bahr, A., Arch. Eisenhuettenw., 30, 489 (1959).

23. Fitzer, E., Chemiker Ztg., 53, 34 (1952).

24. Hartleif, G. and Kornfeld, H., Arch. Eisenhuettenw., 30, 485 (1959).

25. Manterfield, D. and Sykes, W. S., J. Iron Steel Inst. (London), 185, 105 (1957).

26. Masi, O., Met. Ital., 53, 184 (1961).

27. Mathien, V., Rept. Congr. Group. Avan. Methodes Anal. Spectrog. Prod. Met., 19th, 149 (1956).

28. Orsag, J., Rept. Congr. Group. Avan. Methodes Anal. Spectrog. Prod. Met., 18th, 271 (1955).

29. Romand, J., Bachet, C. and Berneron, R., Rev. Met. (Paris), 58, 481 (1961).

30. Romand, J. and Berneron, R., Proc. Colloq. Spectroscopicum Intern., 9th, 2, 325 (1961).

31. Cottenie, A., Congr. Group. Avan. Methodes Anal. Spectrog. Prod. Met., 24, 227 (1962).

32. Amstutz, A. P., Rev. Met. (Paris), 61, 994 (1964).

33. Filimonov, L. N. and Khandros, V. O., Zavodsk. Lab., 24, 712 (1958).

34. Hartleif, G., Stahl Eisen, 78, 837 (1958).

35. Menzies, A. C., Research (London), 14, 285 (1961).

36. Oldfield, J. H., J. Iron Steel Inst. (London), 156, 78 (1947).

37. van Someren, E. H. S., Met. Rev., 7, 329 (1962).

38. Malinek, M., Appl. Spectr., 15, 73 (1961).

39. Patterson, G. D. and Mellon, M. G., Anal. Chem., 24, 131 (1952).

40. Scribner, B. F., Anal. Chem., 30, 596 (1958).

41. Scribner, B. F., Anal. Chem., 32, 229R (1960).

42. Scribner, B. F., Anal. Chem., 34, 200R (1962).

43. Smythe, L. E. and Whitten, R. N., Analyst, 86, 83 (1961).

44. Stadlinger, H., Chemiker Ztg., 77, 287 (1953).

45. Bair, E. J. Introduction to Chemical Instrumentation. New York, McGraw-Hill Book Co. 1962.

46. Malmstadt, H. V., Enke, C. G. and Toren, E. C. Electronics for Scientists. New York, W. A. Benjamin, Inc. 1963.

47. Schottky, W., Ann. Physik, 57, 541 (1918).

48. Brophy, J. J. Basic Electronics for Scientists. New York, McGraw-Hill Book Co. 1966.

49. Engstrom, R. W., J. Opt. Soc. Am., 37, 420 (1947).

50. Oldenberg, O. and Broida, H. P., J. Opt. Soc. Am., 40, 381 (1950).

51. Martinson, O., Isaacs, P., Brown, H. and Ruderman, I. W., Phys. Rev., 79, 178 (1950).

52. Zworykin, V. K., Morton, G. A. and Malter, L., Proc. Inst. Radio Engrs., 21, 351 (1936).

53. Zworykin, V. K. and Ramberg, E. G. Photoelectricity and Its Application. New York, John Wiley and Co. 1949.

54. Condas, G. A., Report 6740, University of California Radiation Laboratory. (1962).

55. Engstrom, R. W., Stoudenheimer, R. G., Palmer, H. L. and Bly, D. A., I. R. E. Trans. on Nuclear Sci., NS-5, No. 3, 120 (1958).

56. Sommer, A. H. and Spicer, W. E., Industry Service Laboratory Report RB-81, Radio Corporation of America (ca. 1951).

57. Electro-Mechanical Research, Inc., Photoelectric Division. [Photomultipliers]. Unpublished material. Princeton, New Jersey, author. 1967.

58. Hughes, A. L. and DuBridge, L. A. Photoelectric Phenomena. New York, McGraw-Hill Book Co. 1932.

59. Eberhardt, E. H., Appl. Opt., 6, 251 (1967).

60. Marrinan, H. J., J. Opt. Soc. Am., 43, 1211 (1953).

61. Boeschoten, F., Milatz, J. M. W. and Smit, C., Physica, 20, 139 (1954).

62. Bronco, C. J., St. John, R. M. and Fowler, R. G., Rev. Sci. Instr., 29, 1145 (1958).

63. Halperin, A. and Kristianpoller, N. K., J. Opt. Soc. Am., 48, 996 (1958).

64. Sluyters, T. J. M. and de Haas, E., Rev. Sci. Instr., 29, 597 (1958).

65. Harman, G. G., Rev. Sci. Instr., 30, 742 (1959).

66. Kolenko, E. A., Protopopov, Kh. V., Fleyshman, D. G. and Yur'ev, V. G., Pribory i Tekhn. Eksperim., 1959, No. 3, 140 (1959).

67. Young, B. M. and Cooper, L. P., Trans. Illumi. Engr. Soc., 24, 46 (1959).

68. St. John, R. M., Rev. Sci. Instr., 32, 370 (1961).

69. Gandy, H. W. and Weller, J. F., Rev. Sci. Instr., 35, 413 (1964).

70. Bay, Z., Rev. Sci. Instr., 12, 127 (1941).

71. Rank, D. H., Pfister, R. J. and Grimm, H. H., J. Opt. Soc. Am., 33, 31 (1943).

72. Blanc-Lapierre, A. and Charles, D., J. Phys. Radium, 5, 239 (1944).

73. Rank, D. H. and Wiegand, R. V., J. Opt. Soc. Am., 36, 325 (1946).

74. Shlyapintokh, V. Y., Vasil'ev, R. F., Karpukhina, O. N., Postnikov, L. M. and Kibalko, L. A., J. Chim. Phys., 57, 1113 (1960).

75. Hutcherson, J. W., Mundy, B. C. and Hefferlin, R., Appl. Spectry., 20, 12 (1966).

76. Tracey, J. E. and Dearborn, F. K., Proc. Cryog. Engr. Conf., 1957, 226 (1957).

77. Young, A. T., Appl. Opt., 2, 51 (1963).

78. Eberhardt, E. H., Research Memo 309, International Telephone and Telegraph Industrial Laboratories (1960).

79. Kaye, W. Fatigue and Hysteresis in Photomultipliers. Unpublished Xeroxed paper presented at Conference on Analytical Chemistry and Applied Spectroscopy, Pittsburgh, Pennsylvania, March, 1967. Fullerton, California, Beckman Instruments, Inc. 1967.

80. Farnsworth, P. T., U.S. Patent 1,773,980. Aug. 26, 1930.

81. Farnsworth, P. T., U.S. Patent 1,941,344. Dec. 26, 1933.

82. Farnsworth, P. T., J. Franklin Inst., 218, 411 (1934).

83. Farnsworth, P. T., U.S. Patent 2,087,683. July 20, 1937.

84. Farnsworth, P. T., U.S. Patent 2,100,841. Nov. 30, 1937.

85. Farnsworth, P. T., U.S. Patent 2,118,186. May 24, 1938.

86. Farnsworth, P. T., U.S. Patent 2,124,057. July 19, 1938.

87. Farnsworth, P. T., U.S. Patent 2,140,695. Dec. 20, 1938.

88. Farnsworth, P. T., U.S. Patent 2,141,836. Dec. 27, 1938.

89. Farnsworth, P. T., U.S. Patent 2,153,918. April 11, 1939.

90. Farnsworth, P. T., U.S. Patent 2,216,265. Oct. 1, 1940.

91. Farnsworth, P. T., U.S. Patent 2,235,477. March 18, 1941.

92. Farnsworth, P. T., U.S. Patent 2,254,140. Aug. 26, 1941.

93. Farnsworth, P. T., U.S. Patent 2,264,630. Dec. 2, 1941.

94. Farnsworth, P. T., U.S. Patent 2,292,111. Aug. 4, 1942.

95. Zworykin, V. K. and Morton, G. A. Television. 2nd ed. New York, John Wiley and Co. 1954.

96. Harber, R. A. and Sonnek, G. E., Appl. Opt., 6, 1039 (1966).

97. Fassel, V. A., Gordon, W. G., Evens, F. M., Altpeter, L. L., Karohl, J. G., Horrigan, V. M. and Skogerboe, R., Proc. Colloq. Spectroscopicum Intern., 8th, 159 (1959).

98. Matsumoto, C., Fassel, V. A. and Kniseley, R. N., Spectrochim. Acta, 21, 889 (1965).

99. Mossotti, V. G. The Atomic Absorption Spectra of the Lanthanide Elements. Unpublished Ph.D. thesis. Ames, Iowa, Library, Iowa State University of Science and Technology. 1964.

100. Chaney, C. L., Spectrochim. Acta, 23A, 1 (1967).

101. Curry, R. H. Flame Spectroscopy of the Rare Earth Elements. Unpublished Ph.D. thesis. Ames, Iowa, Library, Iowa State University of Science and Technology. 1962.

102. Fassel, V. A. and Golightly, D. W., Anal. Chem., 39, 466 (1967).

103. Herrmann, R., Alkemade, C. T. J. and Gilbert, P. T. Chemical Analysis by Flame Photometry. 2nd revised ed. New York, Interscience. 1963.

104. Kaiser, H., Z. Anal. Chem., 209, 1 (1965).

105. Kaiser, H., Z. Anal. Chem., 216, 80 (1966).

106. Harrison, G. R., ed. Massachusetts Institute of Technology Wavelength Tables. New York, John Wiley and Co. 1939.

VII. ACKNOWLEDGMENTS

The author is indebted to Dr. Velmer A. Fassel for his patient guidance and interest shown throughout the course of this study.

Particular gratitude is expressed to Mr. Richard N. Kniseley for valuable suggestions and many enlightening discussions which helped chart the direction of this work.

Also, the author is very appreciative of the masterful work performed by Mr. Gary Wells and Mr. Harry Amenson of the Ames Laboratory Research Metal Shop in the construction of the image-dissector housing. Sincere thanks also go to Messrs. Dean Van Zuuk, Raymond Prior and Dale W. Hilker of the Ames Laboratory Electronics Shop for the design and construction of the electronic focus and sweep supplies.